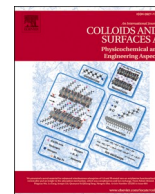




Contents lists available at ScienceDirect

Colloids and Surfaces A: Physicochemical and Engineering Aspects

journal homepage: www.elsevier.com/locate/colsurfa

Application of Pickering emulsions in 3D printing of personalized nutrition. Part I: Development of reduced-fat printable casein-based ink

Mahdiyar Shahbazi^{a,*}, Henry Jäger^{a,*}, Rammile Ettelaie^b

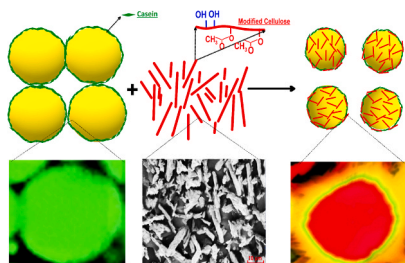
^a Institute of Food Technology, University of Natural Resources and Life Sciences (BOKU), Muthgasse 18, 1190 Vienna, Austria

^b Food Colloids and Bioprocessing Group, School of Food Science and Nutrition, University of Leeds, Leeds LS2 9JT, UK

HIGHLIGHTS

- Pickering emulsions showed thixotropic properties with dynamic and recoverable structure.
- Pickering emulsions displayed structural stability with a thermo-reversible character.
- Emulsions presented a higher amount of nonlinear behavior under large amplitude oscillatory stress.
- Fluorescence images displayed droplets were present in separated and non-flocculated shapes.
- The formation of shear-thinning, viscoelastic, and thixotropic inks by micro-biosurfactant is promising for 3D printing.

GRAPHICAL ABSTRACT



ARTICLE INFO

Keywords:

Surface-active biopolymer
Frequency sweep
Temperature ramp
Thixotropic behavior
LAOS
Creep recovery

ABSTRACT

The application of surface-active biopolymers supports opportunities and novel prospects to generate a well-defined printable ink for 3D printing. In this regard, an ideal ink must show *pseudoplastic*, viscoelastic, and thixotropic characters with a recoverable structure so as to be effectively printed with desired printability. Here, microcrystalline cellulose was hydrophobically modified through a facile and sustainable acetylation method. Then, the functionalized microcrystalline cellulose was incorporated into a casein-based emulsion for being replaced to its partial fat (15–60% fat reduced). The significant effect of micro-biosurfactant on the rheological properties of casein-based emulsion enhanced its shear-thinning, thixotropic, and viscoelastic features. The use of higher ratios of micro-biosurfactant produced an emulsion with greater elastic modulus, smaller droplet sizes, improved stability to the permanent deformation, and increased the nonlinear behavior of the system under large amplitude oscillatory shear stress. The results of the temperature ramp also confirmed the thermo-reversible property of the ink, which was noticeably dependent on the ratios of micro-biosurfactant. The results of this study provided fundamental knowledge about emulsion stability in terms of the contribution of the hydrophobically modified microcrystalline cellulose to interface stability and in promoting resistance to shear stress and deformation. These results allow one to gain a profound understanding of the printability and extrudability of these classes of biomaterials.

* Corresponding authors.

E-mail addresses: shahbazim00@yahoo.com, m.shahbazi1366@gmail.com (M. Shahbazi), henry.jaeger@boku.ac.at (H. Jäger).

<https://doi.org/10.1016/j.colsurfa.2021.126641>

Received 7 March 2021; Received in revised form 9 April 2021; Accepted 11 April 2021

Available online 21 April 2021

0927-7757/© 2021 The Author(s). Published by Elsevier B.V. This is an open access article under the CC BY license (<http://creativecommons.org/licenses/by/4.0/>).

1. Introduction

Increasing demand for modern healthy foods due to changing consumers' attitudes toward healthy lifestyles and industrial strategy in line with the principles of sustainable development are driving the research towards the progress of innovative functionalized products. The processed cheese analogues are homogeneous cheese-like matrices, which are classified into dairy, partial dairy, or non-dairy, relating to the source of the components utilized in their formulation [1]. Compared to natural cheeses, they are cost-effective on account of the application of low-cost vegetable oils rather than milk fat, and the partial replacement of protein by supramolecular biopolymers [2]. Nevertheless, the processed cheeses are often considered unhealthy by consumers because of the high level of fat, which is certainly correlated with a higher prevalence of cardiovascular diseases, obesity, and other diet-related disorders [3]. Thus, scientific works are yielded insights on redesign food toward the development of reduced-fat cheese analogues based on consumer's whims and wishes. Indeed, the elimination of fat impairs the textural, structural, and sensory properties, proposing lower consumer acceptance. In this context, fat replacers can be used as an effective ingredient for calorie reduction to mimic the functional features of fat with consideration of desired textural attributes.

Cellulose, the earth's most abundant bio-based polymer, occurs in the plant cell walls as microfibrillated aggregates and macroscopic fibers, which possess both amorphous and crystalline domains [4]. The amorphous areas inside the microfibrils can be removed through monoprotic, diprotic, or triprotic acids upon controlled hydrolysis circumstance to generate the charged rod-like particles of microcrystalline cellulose (MCC) [4,5]. In principle, the particles of MCC are fairly capable of acting as a stabilizer against coalescence of O/W emulsions rather than against their flocculation or creaming [5]. The MCC is frequently utilized as a suspension stabilizer, thickening agent, fat substitute, and dietary fiber supplement in food products. These functional features have promoted its application in the food sector to prepare sustainable healthy reduced-fat products with a growing number of patents and publications associated with MCC in recent years [5]. Gibis et al. [6] investigated the influence of MCC on the functional features of beef patties, where MCC was compatible with the matrix and improved the textural sensation. Xu et al. [7] evaluated the effect of MCC on the functional features of soybean protein hydrolysate. They reported the negative charge of droplets was increased after MCC addition, offering efficient emulsion stability. Zbikowska et al. [8] replaced MCC with fat in a cookie formulation, in which the content of 25% MCC was the most effective ratio as a substitute for fat.

However, pristine MCC with high surface charge density and poor surface activities is not effective in stabilizing O/W emulsions, thus limiting its wide application as actual interfacial stabilizers. Moreover, both inter- and intramolecular hydrogen bonds simply make the MCC aggregate [9]. The chemical modifications are often applied to reinforce the hydrophobic features of MCC to attain the desired compatibility and interfacial adhesion between MCC and the hydrophobic system. The tuning MCC structure using chemical agents, however, is not a sustainable method, where the process suffers from volatility, toxicity, and instability in the reaction treatment. Thus, a facile and eco-friendly reacting agent from natural resources can be utilized as an effective way to overcome this issue. Acetylation is a frequently utilized method of surface non-polarization in green chemistry and sustainability [10]. It is typically employed to modify the surface of MCC, which proves to be effective in stabilizing O/W emulsions [9–11]. The principle of acetylation is the reaction of the hydroxyl groups of cellulose with an acetyl group, where the obtained surface-active material offers enhanced hydrophobicity, decreased surface polarity, and improved emulsion stability [9,11].

In recent years, rapid prototyping has gained considerable attention in food applications to manufacture custom-designed products, personalized nutrition, and sustainable healthy reduced-fat foods.

Three-dimensional (3D) printing is a promising additive manufacturing technique that offers the rapid prototyping of 3D constructs with consideration of customized and personalized food production. This technique is regularly applied in the engineering of processed cheese [12], semi-hard model cheese [13], casein-whey protein suspension [14], and sodium caseinate-based emulsion [15]. As above-stated, the casein-based cheese-like matrix is a multicomponent complex system and having high moisture content. Thus, it can be sensitive to the thermal treatment and/or extrusion shear forces during the 3D printing process. Once exposed to the constant extrusion force in the 3D printer, the bonds in the cheese-like matrix can be degraded, resulting in a loss of structural integrity [16]. In this regard, diverse ingredients and additives are used to reinforce printable inks to develop a shear-thinning, viscoelastic, and thixotropic character, which offers to maintain the printed structure and capable of adhering to previously deposited layers. An imperative processing way for an effective 3D printing application is the printing of inks in the form of colloidal emulsions or suspensions, which can be stabilized by particulate ("Pickering") emulsifiers. The emulsions that are produced with the irreversible adsorption of micro and/or nanoparticles at the O/W are recognized as Pickering emulsions [17]. Compared to the common surfactant-stabilized emulsions, Pickering emulsion has several benefits, including the requirement of fewer emulsifying agents and greater emulsion stability [17]. This technique has recently attracted extensive attention in the 3D printing process since it is capable of enduring the repeated mechanical deformation during the printing process, achieving enhanced functionality and printability [18–20]. The Pickering emulsion can develop a functional printable ink with enhanced stability against coalescence/flocculation, *pseudoplasticity* feature, and viscoelasticity to be simply squeezed out through the nozzle tip during the printing process [18,20]. Thus, the introduction of surface-active supramolecular polymers possibly enhances the manufacturing speed of printable inks due to the presence of several active binding groups at the interface. This induces the development of a tunable 3D structure with enhanced mechanical performance and printing precision.

Therefore, the main objective of this work was to develop a reduced-fat printable casein-based emulsion formulated with hydrophobically modified MCC. For this purpose, first, the acylated MCC was synthesized by replacing the hydroxyl groups of MCC with acetyl groups of olive oil, and the possible changes in the structural properties of surface-active MCC were investigated. Next, a reduced-fat O/W emulsion with different ratios of micro-biosurfactant was prepared and then instrumental analysis techniques were applied to further prove the effectiveness of Pickering emulsion. For this purpose, rheological properties, temperature ramp, particle size distribution, large amplitude oscillatory shear stress, creep-recovery, three interval thixotropic tests, and confocal laser scanning microscopy with consideration of the functionality of acylated micro-biosurfactant were evaluated.

2. Methods and materials

2.1. Materials

Sodium caseinate (~91% protein, <0.1% calcium content, 3.5% moisture, 0.8% fat, and 0.1% lactose) as the main component was purchased from Fonterra Research and Development Centre (Palmerston North, New Zealand). Microcrystalline cellulose (MCC) Avicel® PH-101, calcium chloride (CaCl₂), analytical grade sodium hydroxide (NaOH), hydrochloric acid (HCl), ethanol, imidazole (C₃N₂H₄), and sodium azide (NaN₃) were supplied by Sigma (Sigma-Aldrich GmbH, Sternheim, Germany). Canola oil, olive oil, and sodium chloride (NaCl) were obtained from a local market and used without additional purification. Cheese flavor agent was obtained from Edlong® (Cork, Ireland). All other reagents used were analytical grade without further purification.

2.2. Surface modification of MCC

MCC was completely dispersed in distilled water (100 g L⁻¹) and stirred using a magnetic stirrer for 120 min at ambient temperature. Then, the MCC suspension was sheared using a high-speed rotor-stator device (Ultra-Turrax, IKA* T25 digital, Germany) for 20 min, which generated a shear force at a shear rate of 210 s⁻¹ (5690 G-force). After completing the process, the sheared MCC was collected and dried in an oven at 40 °C for 36 h. After that, the dried MCC was ground to disrupt the clumps, and filtered by a sieve to attain the particle size of 20 μm.

Acetylation of MCC was carried out using the earlier reported work by Dankovich and Hsieh [21] with some modification. Briefly, a mixture of olive oil (4 g) and 60 mL ethanol was homogenized using an ultrasonic cleaning device (Bandelin 400, Berlin, Germany), operating at 50 kHz for 5 min. Then, the pre-treated MCC (10 g) was incorporated into the homogenous olive oil/ethanol mixture and sonicated again at 50 kHz for 5 min. After the sonication process, the treated MCC was dried at the ambient temperature to complete the elimination of ethanol. The ethanol-free modified MCC was kept in a hot-air oven at 50 °C for 18 h. Next, the functionalized MCC was washed with ethanol for 15 min twice to eliminate the unreacted oil. The functionalized MCC sample was then air-dried and labeled as AMCC.

2.3. Fourier-transform infrared (FTIR) spectroscopy

Transmission infrared spectra of the neat and functionalized MCCs were detected through an FTIR spectrometer (Jasco FT/IR6200, Tokyo, Japan). The solid samples required for the FTIR experiment were attained in the pellet form by mixing about 10 mg of each sample with 100 mg of dry KBr. After that, the specimens were transferred to the pellets to scan the spectral region at the wavenumber ranges of 400 and 4000 cm⁻¹, and 50 scans were recorded with 1 cm⁻¹ resolution [22,23].

2.4. ¹³C nuclear magnetic resonance (¹³C NMR) spectroscopy

To further ensure the hydrophobic modification of MCC structure upon acetylation, ¹³C solid-state NMR was also employed using a Bruker spectrometer (AvanceIII 500, Bruker, Ettlingen, Germany) coupled with a 4-mm magic angle spinning (MAS) probe, in which operating frequency for protons and carbons was 300.13 and 75.46 MHz, respectively. Glycine was utilized as an external reference for the ¹³C spectra and to ensure adjustment to the Hartmann-Hahn matching condition in the cross-polarization tests. The spectra of samples were recorded through the ramp {1 H} → {13 C} cross-polarization (CP)/MAS pulse sequence with proton decoupling upon acquisition. The recycling period was 10 s and a contact time of 3 ms during CP was set for all measurements. The small phase incremental alternation with 64 steps (SPINAL64 sequence) was applied for heteronuclear decoupling during acquisition with a proton field H1H satisfying $\omega_{1H}/2\pi = \gamma_{HH1H} = 62$ kHz. The spinning rate for all the specimens was 10 kHz [11]. The crystallinity index of neat and functionalized MCCs was also obtained by separating the C4 area of the spectrum into amorphous and crystalline peaks, measured by dividing the area of the crystalline peak (96–102 ppm) by the total area assigned to the C4 peak (92–102 ppm), as described elsewhere [24].

2.5. Acetyl percentage and degree of substitution

One limitation of superficial modification is the effectiveness of the substitution. The effectiveness of acetylation was obtained by the acetyl percentage and degree of substitution (DS) through a saponification reaction [25]. The DS is the average extent of acetyl (COCH₃) groups that replaced -OH groups in every glucose unit. The modified MCC (about 1 g) was precisely weighed and then 40 mL of ethyl alcohol (75 v/v%) was mixed with it and stirred at 60 °C for 45 min. Next, 50 mL NaOH (0.5 N) was introduced into the system and stirred using a

magnetic stirrer for 20 min at ambient temperature. A similar method also involved the blank evaluation and back titration with each set of specimens for a control system. The containers were firmly sealed and offered to stand at room temperature for 3 days. The extra alkali in the specimens was titrated via HCl (0.5 N) through phenolphthalein. An excess of approximately 1 mL of HCl was incorporated into the system, which caused NaOH was allowed to diffuse from the sample overnight. The fading of the pink color in the system showed the complete NaOH neutralization. A small amount of HCl was then back titrated with 0.5 N of NaOH until the pale pink color was detected in the system upon strongly shaking the container. The percentage of introduced acetyl group was obtained as follows:

$$\text{Acetyl}(\%) = [(V_4 - V_3)N_{\text{NaOH}} + (V_1 - V_2)N_{\text{HCl}}] \times 4.305/W \quad (1)$$

To measure the DS of the modified MCC, Eq. (2) was defined as:

$$\text{DS} = 3.86 \times \text{Acetyl}(\%)/102.40 - \text{Acetyl}(\%) \quad (2)$$

Here, V_1 = NaOH is volume needed for sample titration; V_2 = NaOH is volume needed for blank titration; V_3 = HCl is volume required for sample titration; V_4 = HCl is volume needed for blank titration; N_{HCl} = HCl concentration; N_{NaOH} = NaOH concentration; W = sample weight.

2.6. Preparation of casein-based Pickering emulsion inks

A buffer solution was made by dispersing 4 mM acetic acid and imidazole into the water and then adjusting the pH to 7.0 through 1 M NaOH. Initial sodium caseinate hydration was done by dispersing powdered sodium caseinate (18 wt%) into 5 mM imidazole/acetate buffer (pH 7.0) and heated to 90 °C and held at this temperature for 1 min, before being stirred at 35 °C overnight to ensure complete hydration. At the same time, the stock suspension of AMCC was prepared by dispersing weighed amount (70 wt% AMCC) of the powdered AMCC into the same buffer (pH 7.0) and homogenized with a high-speed rotor-stator device (Ultra-Turrax T25D IKA, Germany) at a shear rate of 56 s⁻¹ (367 G-force). Then, the AMCC suspension was stirred overnight at room temperature. The pH of this suspension was then adjusted back to pH 7.0.

An O/W emulsion was prepared by blending 10 wt% canola oil and 90 wt% aqueous sodium caseinate (18 wt% sodium caseinate, pH 7.0) using a high-speed blender (Ultra-Turrax T25D IKA, Germany) for 5 min. Simultaneously, 0.3 wt% NaCl was added to the system. This coarse emulsion was then passed through a two-stage high-pressure microfluidizer processor (M110-PS, Microfluidics international Corp., Newton, MA) with 2600 psi at the first stage and 1100 psi at the second stage. The full-fat stabilized emulsion regarded as control hereinafter (10 wt% canola oil, 18 wt% sodium caseinate, pH 7.0) was used to produce reduced-fat emulsions. In this regard, 15%, 30%, 45%, and 60% reduced-fat emulsions were prepared with AMCC stock suspension (70 wt% AMCC, pH 7.0) to yield Pickering emulsions with the following compositions: 8.5 wt% canola oil and 1.05 wt% AMCC (PEC1), 7 wt% canola oil and 2.1 wt% AMCC (PEC2), 5.5 wt% canola oil and 3.15 wt% AMCC (PEC3), and 4 wt% canola oil and 4.2 wt% AMCC (PEC4). In all formulations, the level of sodium caseinate was considered constant (18 wt%). Moreover, the amount of 0.1 wt% cheese flavor agent was added to all formulations. Finally, 0.005 wt% NaN₃ was introduced to the inks as an antimicrobial agent. The finished inks were poured into the plastic containers and stored overnight at 4 °C.

2.7. Rheological experiments of Pickering emulsion inks

2.7.1. Steady rheological properties

The rheological behavior of printable ink variants was characterized by AR 2000ex rheometer (TA Instruments, New Castle, DE) using a parallel plate geometry with a diameter of 40 mm and 1 mm gap. The

Inks were pre-sheared at the shear of 10 s^{-1} for 5 min before start of the experiment cycle. A plastic dropper was used to load samples with the same number of drops. Afterward, the inks were equilibrated at the initial measurement temperature ($30 \text{ }^\circ\text{C}$) for 10 min to reach a steady-state, unless otherwise stated. Shear stress (τ) was determined as a function of increasing shear rate ($\dot{\gamma}$) from 1 s^{-1} – 1000 s^{-1} . The best equation was designated by statistical analysis and the rheological parameters were measured through the optimum model. In this regard, the consistency index, flow behavior index, and yield stress values were measured by fitting the Herschel-Bulkley model (Eq. (3)) to the data:

$$\tau = \tau_0 + K\dot{\gamma}^n \quad (3)$$

where τ is shear stress (Pa); τ_0 is the yield stress (Pa); K is the consistency index (Pa s^n); $\dot{\gamma}$ is the shear rate (s^{-1}), and n is the flow behavior index. The efficiency of the Herschel-Bulkley model was proved by statistical analysis, through residual plots, and normally test with statistical software of Graph Pad In Stat (version 3.05) [26].

2.7.2. Dynamic rheological characterization

Dynamic rheological measurements of the casein-based Pickering emulsions were performed through a AR 2000ex rheometer (TA Instruments, New Castle, DE) using a parallel plate geometry (diameter 40 mm, gap 1 mm). The oscillatory strain sweep (0.1–100%, 1 Hz) was carried out to obtain the limitation of the linear viscoelastic region (LVR). The oscillation stress sweep was also conducted in the mode from 0.1 to 10 Pa (1 Hz) to the upper limit of stress attainable for the rheometer. The values of the oscillatory yield stress of inks were obtained as the crossover point, in which the elastic modulus (G') equals the viscous modulus (G''). Moreover, the frequency sweep experiment (0.1–100 Hz) was investigated in the viscoelastic region ($\gamma = 0.5\%$). All measurements were performed at $30 \text{ }^\circ\text{C}$. The rheological parameters including storage modulus (G'), loss modulus (G''), strain crossover point (γ_c), and frequency crossover point (ω_c) were obtained from the manufacturer supplied computer software (TRIOS, TA Instruments, West Sussex, UK).

2.7.3. Pickering emulsion behavior during heating and cooling

To assess the effect of heating and cooling on the Pickering emulsions, a temperature ramp experiment was conducted through AR 2000ex rheometer (TA Instruments, New Castle, DE) coupled with the Peltier system for temperature control. The ink variants were loaded onto the plate of the rheometer and equilibrated for 4 min before testing. The sweep temperature was applied in the range of 5 – $90 \text{ }^\circ\text{C}$. To recognize the impact of temperature, a range of evaluations was performed through initial conducting a temperature ramp (heating) from $5 \text{ }^\circ\text{C}$ to $90 \text{ }^\circ\text{C}$ and a time sweep test at $90 \text{ }^\circ\text{C}$ for 10 min, followed by a temperature ramp (cooling) from 90 to $5 \text{ }^\circ\text{C}$, and a time sweep at $5 \text{ }^\circ\text{C}$ for 10 min. The entire cycle was repeated once to assess the reversibility of the system. All measurements were performed at 50% of the smallest critical strain determined (0.5%) and a frequency of 1 Hz.

2.7.4. Creep and creep-recovery test

The creep and creep recovery compliance of Pickering emulsions represent the viscoelastic response of microstructure to the constant applied shear stress and elimination. The creep is considered as the slow development of strain at the applied constant shear stress. The creep-recovery assay was conducted to measure the compliance level in the creep and recovery stages. In this regard, the stress sweep (1 Hz, 0.1–10 Pa) was performed to determine the oscillatory yield stress. Next, the shear stress values applied for the ink variants were considered as about 50% of the oscillatory yield stress ($G'(\tau) = G''(\tau)$). The inks were transferred into the parallel-plate flow chambers (diameter 40 mm, gap 1 mm) at $30 \text{ }^\circ\text{C}$. The creep measurement involved the application of prompt and constant shear stress inside the LVR area, from 0 to 1000 s, while measuring the sample strain between time intervals. Concerning

the recovery stage, the applied stress was rapidly eliminated ($\tau_{\text{applied}} = 0.0 \text{ Pa}$) and the ink recovery was recorded for an additional time of 1000 s at the same temperature in the creep phase. The recovery value was measured immediately after the finishing of the creep phase. The time interval was detected to be proper for the ink variants to achieve the steady strain extents. The calculated strain and recovery were taken as the creep compliance and creep recovery compliance (J) (Eq. 4). The creep recovery percentages of Pickering emulsions were then calculated according to Eq. (5):

$$J(t) = \gamma(t)/\tau_0 \quad (4)$$

$$\text{Percentage recovery} = (J_m - J_e)/J_m \times 100\% \quad (5)$$

where $J(t)$ (Pa^{-1}) is creep compliance, γ is the measured strain, t is time, τ_0 is the constant applied shear stress, J_m (Pa^{-1}) is the maximum creep, J_e (Pa^{-1}) is the equilibrium creep compliance after recovery.

2.7.5. Three interval thixotropy test (3ITT)

The 3ITT experiment was applied to assess the time-dependent nature of the Pickering emulsions and recovering capabilities of the initial structures during utilization of low-shear rate after high-shear circumstances. The 3ITT involved a three-step shear rate experiment, in which the first one included a steady shear rate to identify the ink reference stage without interrupting the microstructure using a fixed shear rate of 1 s^{-1} for 400 s. This was followed by the second interval, where a steady shear rate of 80 s^{-1} for 200 s was used to disrupt the microstructure of the ink. The third interval comprised a comparable test condition as the first interval, obtaining the reversible recovery of the structure of Pickering emulsions.

2.8. Large amplitude oscillatory shear stress (LAOS)

The LAOS assay was performed by a Discovery Hybrid Rheometer (DHR3, TA Instruments Inc., New Castle, DE) equipped with a cone-plate geometry (diameter = 40 mm, cone angle = 1°). A solvent trap was used to avoid water evaporation from the inks during the measurements. The LAOS experiment was then performed at $30 \text{ }^\circ\text{C}$ by collecting raw waveform results at 0.5%, 50%, and 100% strains at three different frequencies of 0.5, 5, and 10 Hz. Then, the Lissajous-Bowditch plots of Pickering emulsions at different amplitude and frequencies inside and beyond the LVR were obtained.

2.9. Determination of droplet size

To prevent the multiple scattering impacts, the Pickering emulsion droplets in printable inks were diluted to a droplet concentration of about 0.005 wt% using imidazole/acetate buffer solution at the pH of Pickering emulsions (pH = 7.0) and stirred constantly through the experiment to ensure the inks were homogenous. The droplet sizes and particle size distribution of the Pickering emulsions were obtained through a laser diffraction instrument (MS2000, Malvern Instruments Ltd., Worcestershire, UK). The device measures size based on the scattering of a monochromatic beam of laser light ($k = 632.8 \text{ nm}$). The droplet size was stated as the surface-weighted mean $d_{(3,2)} = (\sum n_i d_i^3 / \sum n_i d_i^2)$ and volume mean diameters $d_{(4,3)} = (\sum n_i d_i^4 / \sum n_i d_i^3)$, in which n is the number of droplets with diameter d_i .

2.10. Determination of zeta potential (ζ -potential)

The electrical charges (ζ -potential) of the printable inks were obtained through a Zetasizer Nano-ZS90 (Malvern Instruments, Worcestershire, UK) at a fixed detector angle of 90° . The Pickering emulsions were diluted by imidazole/acetate buffer solution to a final concentration of 0.005 wt% before each measurement to minimize the multiple scattering effects. After loading the inks into the chamber of the Zetasizer,

they were equilibrated for 5 min before ζ -potential data was obtained from 40 continuous readings.

2.11. Confocal laser scanning microscopy (CLSM)

The network structure and interfacial framework in the continuous phase of the casein-based inks were detected through CLSM. Precisely, five mL of ink-stained with the appropriate amount of Nile Blue A (1.0%, w/v) in distilled water, or the mixture of Nile Blue A (1%, w/v) and Nile Red (0.1%, w/v) in 1,2-propanediol (containing distilled water, $20 \mu\text{L g}^{-1}$) were used to mark the protein and/or functionalized MMC and oil droplet, respectively. The amount of both Nile blue A and Nile red solution was 0.01% (w/v). The excitation wavelengths of fluorescent in the system were 488 nm (Nile red) and 633 nm (Nile blue A). The morphology of the ink microstructure was captured at room temperature directly after staining via an FV-300 confocal scanning instrument (Olympus, Tokyo, Japan) coupled with an Olympus IX71 inverted microscope and an argon-ion laser. All images were obtained at $40\times$ magnification and processed using Olympus Fluoview software.

2.12. Statistical analysis

All instrumental experiments were carried out as triplicate determinations and the mean and standard deviation of the data were reported. Analysis of variance (ANOVA) was utilized for the determination of the main effects of the examined independent factors and their interactions on the instrumental data. Duncan's multiple range test was applied to separate means of data when significant differences ($P < 0.05$) were observed.

3. Results and discussion

3.1. Characterization of synthesized acetylated MCC

The possible mechanism for surface esterification of MCC induced by acetyl groups is schematically proposed in Fig. 1a. Moreover, Fig. 1b shows the scanning electron microscopy (SEM) photograph of AMCC, where the particles are similar in size and morphology, well-separated from each other, and no obvious agglomeration was observed (for interpretation of the reference to the preparation of AMCC for SEM analyze, the reader is referred to the [Supplementary Materials](#) of this

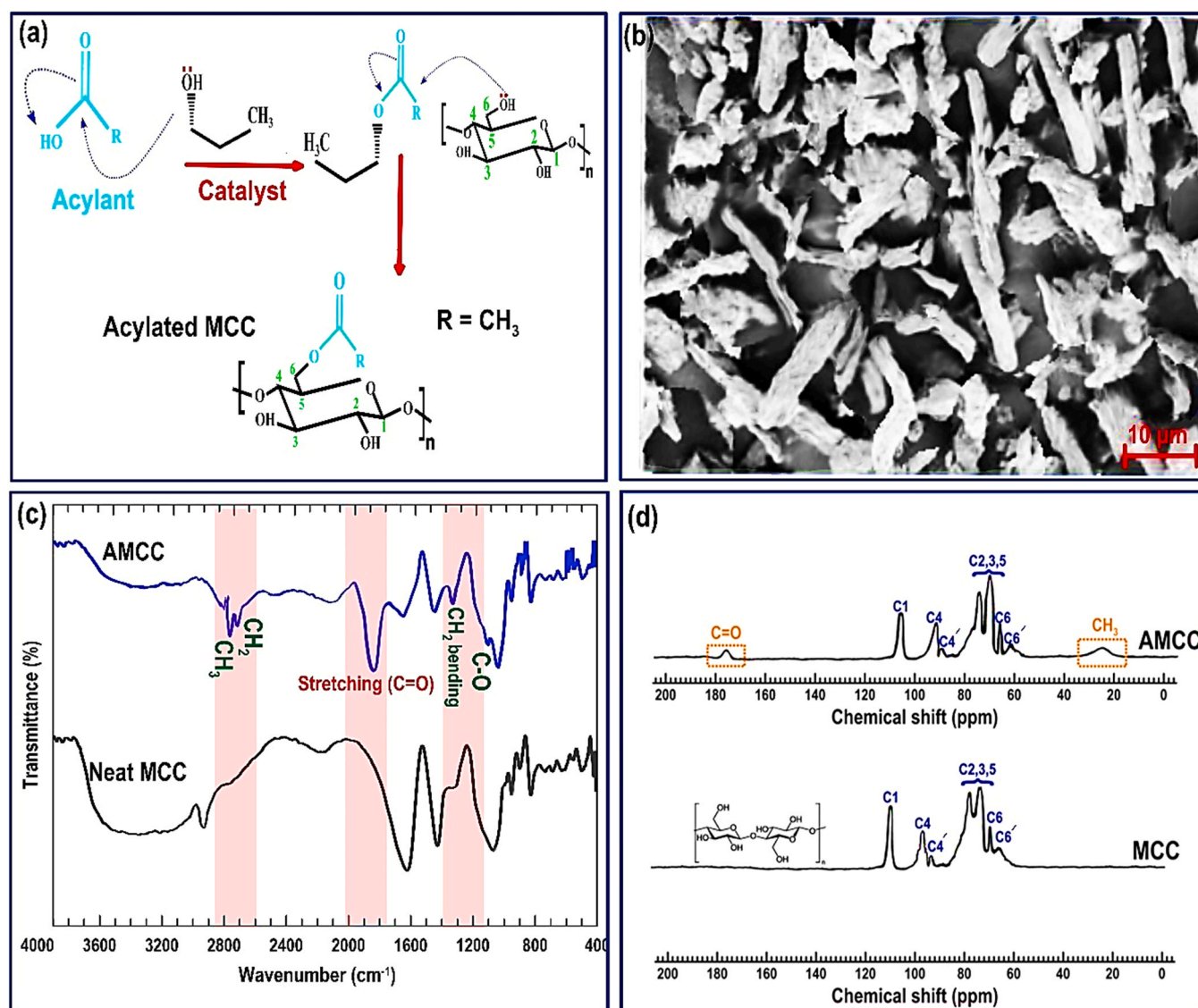


Fig. 1. (a) Schematic of the possible mechanism of MCC esterification through acetylation. (b): SEM micrograph of synthesized AMCC. (c): FTIR spectra and (d): ¹³C solid-state NMR of pristine and acetylated MCCs.

article). The degree of substitution assay also revealed that AMCC showed a DS value of 1.9 with a crystallinity index of ~84% obtained by ^{13}C NMR. The FTIR spectra of unmodified MCC and its acylated product are illustrated in Fig. 1c. The typical characteristic vibration of unmodified MCC showed the distinguished bands of cellulose I at about 2800 cm^{-1} – 3750 cm^{-1} and 600 cm^{-1} – 1750 cm^{-1} . In this case, the peak at 3389 cm^{-1} was attributed to the stretching of the -OH group. Besides, other characteristic peaks were included as C-H stretching (2936 cm^{-1}); asymmetric stretching vibration of COOH groups (1637 cm^{-1}); CH_2 symmetrical bending (1426 cm^{-1}); cellulose C-O-C bridges (1075 cm^{-1}); ether C-O-C functionalities (962 cm^{-1}); and the band at 876 cm^{-1} , which is typical of β -linked glucose polymer [11]. In the case of acetylated MCC (i.e., AMCC), a new strong carbonyl stretching vibration at 1832 cm^{-1} (C=O) was easily identified [10]. At the same time, the intensity of the stretching peak of the -OH group was broader and more subdued. This might be due to the replacement of the hydroxyl groups of MCC by acetyl groups of olive oil through acetylation (Fig. 1a). The AMCC sample also showed four new characteristic peaks regarding methyl (2791 cm^{-1}) and methylene (2704 cm^{-1}) stretching vibrations, $-\text{CH}_2$ bending at 1362 cm^{-1} , and carbonyl stretch vibration (C-O) at 1108 cm^{-1} . A similar absorption pattern was also reported by Lin et al. [9] and Kale et al. [10]. The absence of absorption at 1637 cm^{-1} (attributed to carboxylic groups) indicated that no unreacted acetylant remained in the esterified MCC. These changes showed that the hydroxyl groups of MCC were covalently bonded with acetyl chains of triglycerides in the olive oil during the acetylation reaction process.

The esterification of MCC was further qualitatively confirmed by ^{13}C solid-state NMR spectroscopy (Fig. 1d). The unmodified MCC spectrum revealed the typical carbon peaks of cellulose I, i.e., C1: 111.2 ppm, C4: 97.8 ppm, C4': 94.7 ppm, cluster C2-C3-C5: 71.7–79.2 ppm, C6: 70.2 ppm, and C6': 65.3 ppm [27]. As the esterification reaction proceeded, several new resonances appeared on the spectrum of AMCC. In this regard, a new rather broad peak was observed at 176.9 ppm, relating to the resonance of the carbonyl ester peak. The AMCC also showed the appearance of a new wide signal at 24.3 ppm, which arose from the terminal methyl carbons of acetylant [11]. The crystalline and disordered components of unmodified MCC were calculated in the solid-state ^{13}C NMR spectra as downfield and upfield lines for the C4 or C6 carbons, respectively [24]. As Fig. 1d shown, the unmodified MCC presented a wide non-crystalline resonance centered at 84 and 62.7 ppm (upfield lines, i.e., C4' and C6', respectively). Downfield signals centered at 92 and 65.3 ppm (C4 and C6, respectively) have been assigned to the ordered cellulose structures [24,27]. The crystallinity index of unmodified and acetylated MCCs was then calculated using the peak separation method [28] by dividing the area of the crystalline peak using the total area assigned to the C4 peaks. The obtained crystallinity index values suggested that no significant change in the crystallinity of MCC (~84%) took place during esterification.

3.2. Characterizations of casein-based Pickering emulsion inks

3.2.1. Flow curve

The steady rheological feature of the printable inks was obtained as it can provide useful insights into the flow behavior of systems, which directly affects the printability and shape fidelity [16]. All the flow curves were fitted to the Herschel-Bulkley model with high correlation coefficients (R^2) above 0.980. The consistency index (K), yield stress (τ_0), and flow behavior index (n) (derived from the Herschel-Bulkley model) for the ink variants are given in Table 1.

The flow curve was provided via plotting the recorded viscosity and shear stress as a function of the applied shear rate (Fig. 2a). The non-linear increase in the shear stress with increasing shear rate specified that all inks displayed a shear-thinning character. Compared to control, the Pickering emulsion containing 1.05 wt% AMCC (PEC1) showed an appreciable increase in the shear stress with shear rate (Fig. 2a). However, it showed small yield stress (0.72 Pa), a moderately low

Table 1

Summary of obtained consistency index, flow behavior index, and yield stress of different ink samples.

Samples	Yield stress (Pa)	Consistency index (Pa s^n)	Flow behavior index	R^2
Control	0.71 ± 0.01^a	1.13 ± 0.02^a	0.882 ± 0.006^d	0.981
PEC1	0.72 ± 0.01^a	1.50 ± 0.03^b	0.876 ± 0.003^d	0.984
PEC2	0.79 ± 0.03^b	1.94 ± 0.04^c	0.831 ± 0.002^c	0.982
PEC3	1.92 ± 0.01^c	3.41 ± 0.06^d	0.716 ± 0.003^b	0.983
PEC4	2.64 ± 0.01^d	4.25 ± 0.05^e	0.652 ± 0.001^a	0.986

^{a-e} Means (three replicates) within each column with different letters are significantly different ($P < 0.05$), Duncan's test.

consistency index (1.50 Pa s^n), and some shear-thinning ($n = 0.876$) (Table 1). This might be attributed to a lower level of free AMCC to cover the oil droplets in the system. Moreover, it could be denoted the volume fraction of micro-biosurfactant in the emulsion might be lower than the close-packing limit, if not PEC1 ink would have had a great viscosity and yield stress [29]. The rheological data also revealed that PEC2 offered a non-linear increase in the shear stress with shear rate, however, compared to PEC1 showed a somewhat higher consistency index (1.94 Pa s^n), greater yield stress (0.79 Pa), and some shear-thinning ($n = 0.831$). The greater yield stress and consistency index suggested that the micro-biosurfactant was in the area where some biopolymeric overlaps occurred, leading to fairly high viscosity and shear-thinning [29]. Table 1 also shows that introducing higher levels of AMCC into the system (3.15 and 4.2 wt%) caused a noticeable decrease in the flow behavior index, indicating the emulsion became more shear-thinning. This could be a sign that the aggregated droplets break into smaller clusters under increasing shear, causing shear-thinning. Besides, at the higher AMCC ratios, a much more increase in the shear stress with the shear rate was detected (Fig. 2a). This result was expected since there are more hydrophobic/hydrophilic groups offered by micro-biosurfactant to interact with comparable groups in the adjacent droplets, subsequently increasing shear stress with shear rate. The extent of the consistency index also substantially increased as the AMCC level was increased (Table 1). The important increase in this parameter with increasing micro-biosurfactant ratio might be primarily associated with two main effects: (i) the micro-biosurfactant particles themselves contributed to the overall disperse phase volume fraction of the dispersion; (ii) the existence of intermolecular interactions between hydroxyl/acetyl groups of AMCC and hydrophilic/hydrophobic domains of casein/oil phases, respectively [30]. Likewise, the fact that a notable increase in the yield stress was noted regarding PEC3 and PEC4 (Table 1) proposed the development of the initiation of individual chains overlap and formation of a three-dimensional network. In this sense, the existence of a high level of yield stress with more shear-thinning character can be desirable for 3D printing purposes, in which printable inks must be capable of being poured or spread, but should preserve their shape upon extrusion force in the 3D printer [16].

3.2.2. Strain sweep

The flow behavior of printable ink has been specified as the principal property aimed at the printing purpose. The flow behavior alone, however, cannot capture the complex behavior of inks upon the 3D printing process. The oscillatory shear tests are regularly utilized to simultaneously evaluate the viscoelastic parameters of printable ink. It is reported that a viscoelastic character can offer inks to efficiently preserve their geometrical structures during the printing process, especially providing advantageous features required to construct the intricate architectures [16]. The storage (G') and loss (G'') moduli of different inks as a function of oscillatory amplitude sweep are shown in Fig. 2b. Regardless of ink type, the G' amounts remained nearly constant until a critical strain was attained and then fell abruptly, which is revealing a breakdown of the crosslink networks in the system. All the ink variants showed $G'(\gamma) > G''(\gamma)$ for a large range of strain amplitudes (<10%) that

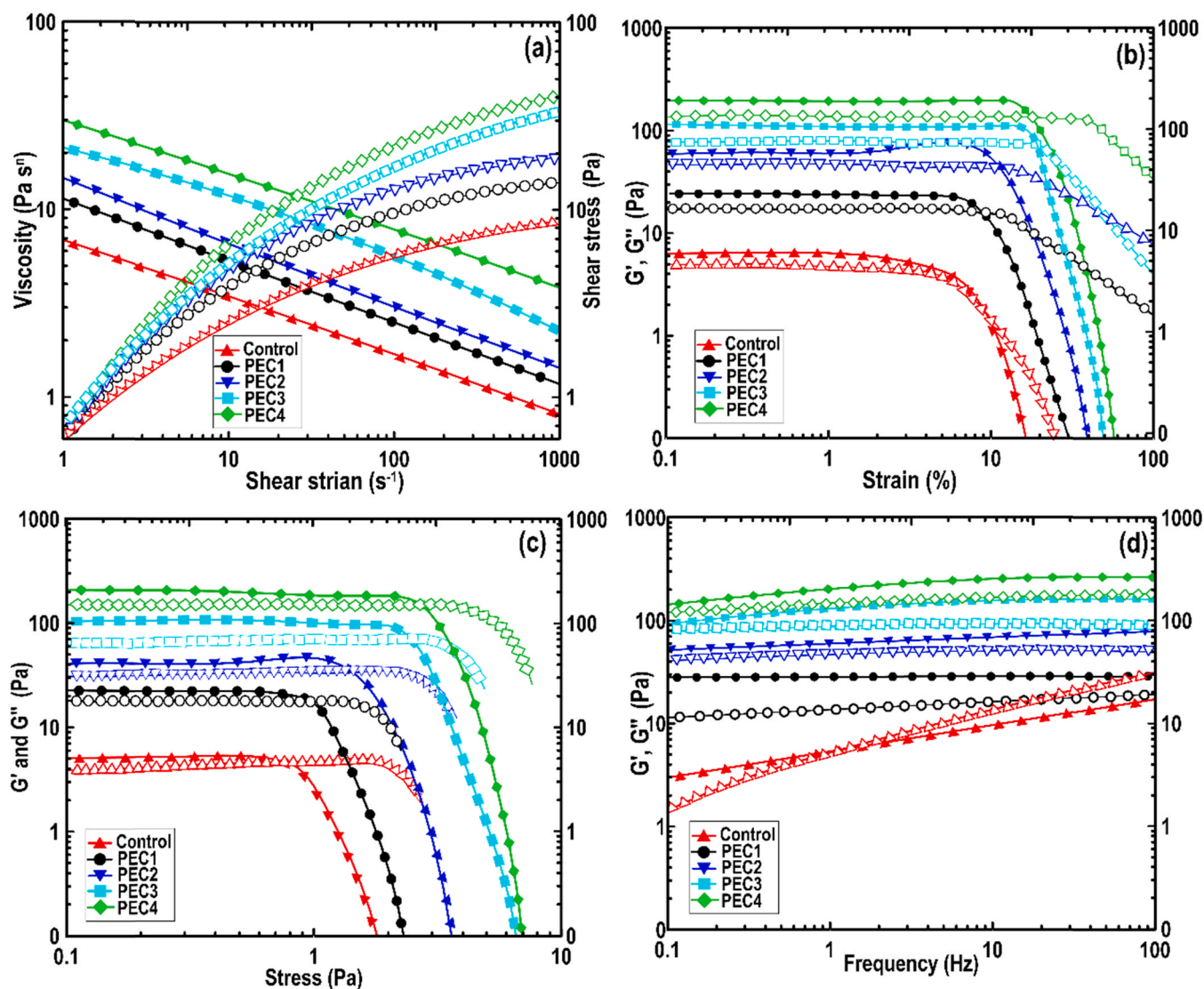


Fig. 2. (a) Changes in viscosity and shear stress as a function of applied shear rate in different samples. (b): Amplitude sweep, (c): stress sweep, and (d): frequency sweep of casein-based emulsions, where G' is solid symbols and G'' is open symbols.

is indicative of the elastic or solid-like behavior of the system. The G' parameter provides an indication of the system firmness, in which higher G' may offer an improvement of the ink functionality with consideration of printing precision, resolution of deposited layers, and consequently, developing a well-defined geometry [16]. At the entire stage of amplitude sweep, the reduced-fat inks revealed a higher viscoelastic parameter compared to control ink. This might be originated from the presence of intermolecular interactions between the polar cellulose chain ends and acetyl groups of AMCC with hydrophilic and hydrophobic domains of the casein/oil system, respectively. Besides, as demonstrated by the steady flow profile, the reduced-fat inks presented an emulsion with a larger consistency index and higher yield stress. In general, the $G'(\gamma)$ of PEC1 was somewhat higher than control ink, followed by PEC2 and PEC3. The PEC4 displayed the greatest $G'(\gamma)$ value, indicating the formation of a more structured and stable system with an improved connected matrix. In the presence of higher levels of micro-biosurfactant, the initiation of biopolymeric coils overlap, and the development of intermolecular junctions in the system might limit the elongation and arrangement of the polymeric chains [29]. For the purposes of this study, the Pickering emulsions that offered higher elastic behavior and strong gel-like structure were considered as an appropriate

dispersion and may be utilized as the printable ink for further investigations.

To guarantee the operating circumstances inside the viscoelastic region and to assess the structural features of the protein network, the change in the LVR length was also taken into consideration. The LVR signifies the range of oscillatory amplitude within which the ink structure was stable and remained constant. The length of LVR also indicates the strength of structural stability of the system, where the strong emulsions may remain in the LVR over a higher deformation rate than the weak system [31]. The limit of LVR was represented as the point in which the viscoelastic variables do not differ by an appreciable magnitude from a constant amount (5%), and therefore was considered as the critical strain [31]. Regardless of ink type, the $G'(\gamma)$ magnitudes progressively reduced above the critical strain, demonstrating a transition of the systems from the quasi-solid phase to a quasi-liquid state (Fig. 2b). Within LVR, the $G'(\gamma)$ parameters of the ink variants were principally independent of the applied strain amplitude, acting like a viscoelastic solid. According to oscillatory amplitude sweep data, control ink showed a shorter LVR length with a lower critical strain value (1.6%) compared to the reduced-fat inks. The extents of critical strain regarding PEC1, PEC2, PEC3, and PEC4 were determined to be 6.8%, 11.4%, 18.1%, and

27.3%, respectively. Accordingly, the $\gamma = 0.5\%$ was considered in the following oscillation experiments to ensure the subsequent dynamic oscillatory deformation of each ink inside LVR. The critical strain is directly assigned to the molecular structure of the polymeric chains along with the deformability of the systems, in which emulsions with higher critical strain preserve their viscoelasticity character for a longer LVR length [31]. As a consequence, compared to the lower micro-biosurfactant ratio, the inks including higher levels of AMCC presented a comparatively higher G'_{LVR} and longer LVR, and therefore a higher critical strain.

The loss modulus (G'') is generally associated with the energy dissipation upon deforming, which is assigned to the degradation and reorganization of the network and slippage of the polymeric chains. As Fig. 2b depicted, the trend of the $G''(\gamma)$ curve was clearly different before and after micro-biosurfactant addition. At the initial stage of the strain sweep, *i.e.*, within LVR, the magnitudes of $G''(\gamma)$ were almost constant for all inks. However, a maximum at the higher amplitude sweep ($>10\%$) was noticed regarding reduced-fat inks, in which $G''(\gamma)$ curves crossed over with those of G' (*i.e.*, $G' = G''$) (Fig. 2b). The presence of a maximum in the $G''(\gamma)$ was considered as the type III phenomenon (weak strain overshoot), observing in the soft glassy compounds, structured emulsions, entangled biopolymeric emulsions, and associative biopolymeric systems [32]. The peak in $G''(\gamma)$ indicated maximum energy dissipation and the crossover (γ_c) of viscoelastic moduli showed a transition from viscoelastic solid-like to viscoelastic liquid behavior. Compared to control, a shift in the γ_c point to the higher amplitude sweep was noticed for the reduced-fat inks, showing the promotion of a more structured system with a strong gel-like structure. Following that transformation, the constant decrease of $G'(\gamma)$ or $G''(\gamma)$ presented the rigidity of systems was decreased by increasing the strain amplitude. The important reason for the descended oscillatory viscoelastic parameters is the disentanglement of the polymeric structure [31]. As an outcome, the desired printable ink should be able to maintain the structured ordering upon extrusion shear force and also fusing with previously 3D printed layers. Accordingly, an improvement in the viscoelastic parameters of reduced-fat inks offered by higher ratios of AMCC might provide structural stability during printing and also better holding their 3D structures after the process.

3.2.3. Stress sweep test

Fig. 2c shows the evolution of viscoelastic parameters of Pickering ink variants as a function of the applied oscillation stress. In all samples, $G'(\tau)$ was higher than $G''(\tau)$ at the low shear rate (<1 Pa), which offered a typical gel-like structure. It is obvious from the stress sweep graph that with increasing the ratios of micro-biosurfactant, both moduli were shifted toward the higher values. Regarding $G'(\tau)$, as the sign of system stiffness, it could be stated that the structure of Pickering emulsion was strengthened as the ratio of AMCC increased. Fig. 2c also displays that upon micro-biosurfactant incorporation, the length of the LVR, *i.e.*, the stress range inside which no structure breakdown occurs, became longer. Additionally, at a certain point, $G'(\tau)$ was equal to $G''(\tau)$. This is the intersection of the elastic and viscous behaviors and is considered as the oscillatory yield stress [31]. Further increase in the applied oscillation stress led to $G''(\tau)$ values became higher than $G'(\tau)$, displaying the viscous behavior of the system. The stress sweep results also indicated that the oscillatory rheology was capable to capture the differences in the yield stress of Pickering emulsions, which provided a good estimate of static yield stress obtained by the Herschel-Bulkley model.

3.2.4. Frequency sweep

The elastic and viscous parameters as a function of oscillatory frequency (ω) for printable inks inside the LVR are depicted in Fig. 2d. It is obviously detected that $G'(\omega)$ or $G''(\omega)$ of the reduced-fat inks basically followed by a comparable trend. In this regard, the elasticity of these samples is further apparent from the fact that the $G'(\omega)$ or $G''(\omega)$ values were slightly sensitive to the angular frequency, which specified the

reduced-fat ink systems developed a stable network structure. Regarding control ink, quasi-solid behavior was dominating at the low frequencies (<1 Hz), where $G'(\omega) > G''(\omega)$. However, as the frequency proceeded, there was a regional monotonic increase in moduli, where the $G''(\omega)$ was gradually getting closer to $G'(\omega)$ until a crossover point (ω_c), *i.e.*, $G'(\omega) = G''(\omega)$. This suggests the breakdown of polymeric chains and the destruction of the polymeric interactions and the formation of a typical liquid-like system [31,33]. On the other hand, the moduli of the reduced-fat inks showed a fairly linear increase with an increase of angular frequency, but the slope of $G''(\omega)$ was always lower than $G'(\omega)$ throughout the frequency sweep test, representing a gel-like behavior. This denotes the $G'(\omega)$ values of all reduced-fat inks dominated $G''(\omega)$ and no ω_c point was observed at frequencies from 0.1 to 100 Hz. Besides, the magnitudes of $G'(\omega)$ were notably increased with increasing the ratio of AMCC. This is possibly emphasized the induction of a strong gel-like network in the system. In the presence of higher ratios of micro-biosurfactant, there are more acetyl groups and cellulose backbone to interact with the comparable groups in the adjacent droplets, where they might be more efficiently dispersed and less aggregated. The reinforcing effect of AMCC was also reflected on $G''(\omega)$, whose values linearly increased through the frequency sweep range. This offers the improved stability of inks, presenting more structured and connected networks since the inks acted as an elastic gel-like system. The development of a viscoelastic Pickering emulsion, offered by higher levels of micro-biosurfactant, might be valuable for a printed structure to keep its shape upon application of extrusion forces in a 3D printer. This can improve the printability and printing accuracy of a 3D printed construct.

3.2.5. Temperature-controlled rheometry

For many practical applications of the 3D printing technique, it is critical to determine how printable inks behave under different processing temperatures with various holding times. The behavior of ink variants upon heating and cooling was investigated by subjecting the Pickering emulsions to the temperature-controlled rheometry. The dependence of complex modulus (G^*) (as an index of the system rigidity) on the temperature sweeping is exhibited in Fig. 3a. Four phases of G^* transitions were detected in all emulsions: 1) heating and holding at 90 °C, 2) cooling to 5 °C and holding for 10 min, 3) heating to and holding at 90 °C, and 4) cooling to 5 °C and holding for 10 min. In general, the curves of reduced-fat inks presented a qualitatively similar trend, but with important quantitative differences. At the initial phase of the thermal treatment ($T < 55$ °C) a sharp reduction in the G^* took place. This phase was occurred in all Pickering emulsions and included a slight increase in the polymeric movement because of thermal agitation. In this sense, some extent of hydrogen linkages might be weakened, but partial protein aggregation is also possible. From literature, hydrogen interaction is not the only force for protein aggregation and other protein conformations, but it could act as the main interaction force in protein structural stabilization [34]. In general, the inks formulated by the higher levels of AMCC offered a greater G^* value. This might be on account of the stabilizing effect of micro-biosurfactant either due to an increase in the viscosity of continuous phase or promotion of a gel-like structure. The first phase was followed by an obvious increase in G^* parameter ($50 < T < 65$ °C), except for PEC3 and PEC4 inks (Fig. 3a). The increasing trend of G^* displayed an affinity to the asymptotic value during the first heating ramp, which is in accordance with the study for the heat-induced protein [35]. In the current work, a peak in the G^* could be likely due to an increase in the system entropy as a consequence of protein aggregation with a less ordered state. It might be also associated with the structural changes of the different segments of casein micelles, which led to the segmentation motion of the polymeric strands [36]. As above-stated, the increasing trend of G^* through the initial heating phase did not detect in the inks containing 3.15 and 4.2 wt% AMCC, in which they had an obvious decreasing trend with temperature. The formation of comparatively tough structure could be as a result of linkage between hydrophilic groups of micro-biosurfactant with the

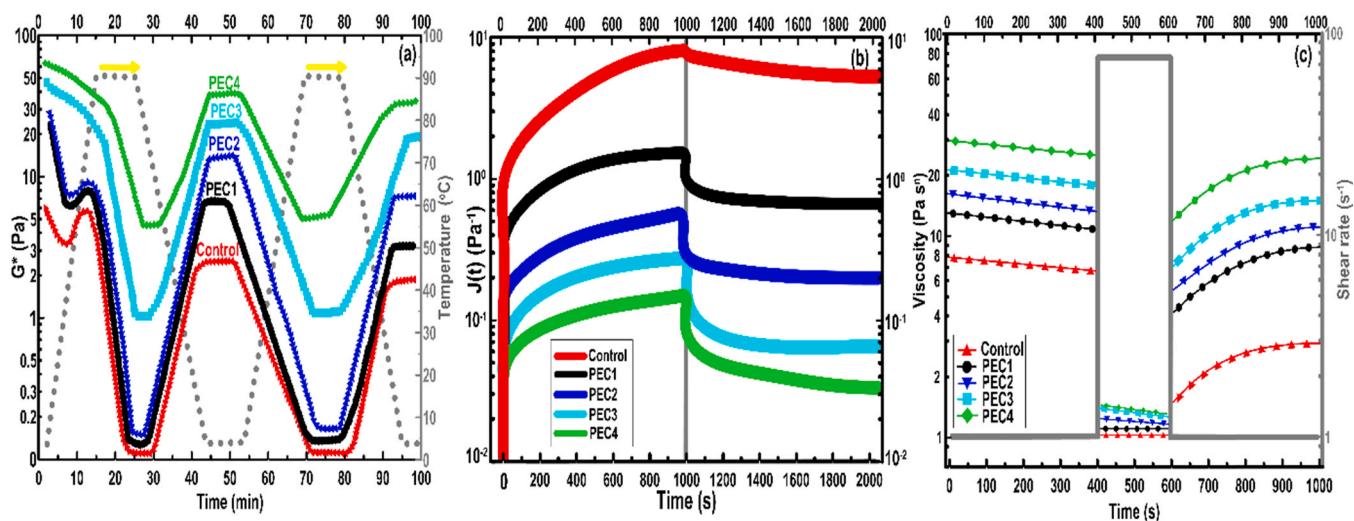


Fig. 3. (a) Temperature ramp curves of Pickering emulsion variants plotted as G^* versus time. (b): Creep and creep-recovery curves and (c) the 3-ITT of prepared Pickering emulsion variants.

polar groups of casein backbone, where more hydrophilic groups were consumed through intermolecular interactions. This made the structure of PEC3 and PEC4 inks to be much firmer than those of other Pickering emulsions.

Fig. 3a also shows that a further increase in the temperature to 90 °C resulted in a sharp decrease in G^* values. The degradations of some weak chemical linkages and losing much more hydrogen bonding were all in this state to obtain a decreased G^* trend, causing a loss of structural integrity and stability of the system. However, regarding PEC3 and PEC4, the G^* value was decreased by a slight downward slope. This shows the development of strong intermolecular interactions between functional groups of AMCC and casein/oil, offering a structured network system. During holding at 90 °C, control ink attained a constant lowest G^* level, signifying the sol-state nature of this sample. For this stage, the reduced-fat inks showed a noticeably higher G^* compared to control, in which the PEC4 offered the greatest G^* level. A higher value of G^* in all inks occurred at the first cooling phase, giving rise to the equilibrium amounts as the temperature of 5 °C was maintained. It is reported that the aggregation of the casein micelles upon heating is initially, at least partially, reversible [36]. The physical linkages, mostly the hydrogen interaction, might be responsible for this evolution. The hydrogen interactions among the amino acids and water molecules or between the adjusting biopolymeric strands mainly developed upon the cooling phase. This could be imperative in the stabilization of the protein system. In this context, the hydrogen bonds also contribute to immobilizing water into the hydrogel network, promoting the gelation upon cooling the inks to 5 °C. It was observed that the gelation time of PEC3 and PEC4 was also increased, albeit with a gentle slope (Fig. 3a). This is possibly due to the promotion of more intermolecular interactions offering by the higher ratios of AMCC, which hindered the rearrangements and aggregation of the casein networks.

On the second heating phase (re-heating) of inks to 90 °C, the G^* values showed a progressive reduction, suggesting the melting and gel-sol transformation (Fig. 3a). The temperature ramp findings suggested the G^* values of reduced-fat inks less decreased than the control sample. Moreover, the decreased G^* level was also small for PEC3 and PEC4, while concerning PEC1 and PEC2 the decrease in G^* was sharper and occurred earlier for the lower temperatures. This denotes the development of a properly connected structure in the case of PEC3 and PEC4 with a reinforced gel strength (higher final G^*). The G^* of inks recovered to the equilibrium plateau state on the second phase of cooling to 5 °C, therefore confirming the thermo-reversible character of the casein-based Pickering emulsions. Generally, under these conditions, the

presence of surface-active MCC showed a positive impact on the gel formation, increasing the rate of structure development with an improved gelation temperature, which was clearly dependent on the levels of micro-biosurfactant. As a consequence, the structure of reduced-fat inks (during heating, holding, and cooling phases) was retained throughout the evaluated temperature profile, confirming the reduced-fat inks were thermostable. After the completion of the temperature sweep experiment, the G^* of control ink decreased nearly five-fold owing to the heating degradation of the weak biopolymeric network. On the contrary, the reduced-fat inks, especially the inks with higher AMCC ratios, still somewhat preserved their microstructure with little evidence of the heating breakdown. Considering the temperature impact on the structural integrity, the results seemed to suggest the presence of both hydrophobic and hydrophilic interactions in the system, which get stronger with introducing greater ratios of micro-biosurfactant. In this context, PEC3 and PEC4 inks revealed larger structural recovery compared to the rest of Pickering emulsions, offering an increased structural stability due to developed intermolecular interactions between the functional groups. This can be an advantage in the printing process, where these inks might have shown good thermal stability and high resistance against any extrusion shear force in the printer, improving its durability upon the printing process.

3.2.6. Creep recovery measurement

Another imperative factor in the ink flow behavior measurement is a creep and creep-recovery evaluation, which is beneficial to perform a dispersion with data from empirical approaches. The thixotropic feature of inks was conducted by investigating the viscoelasticity of the Pickering emulsions through a creep and creep-recovery test (Fig. 3b). This experiment includes the utilization of constant applied shear stress; when the stress is removed, the viscoelastic compound displays a recovery to its initial shape or a progressive reduction of deformation over time. The viscoelastic feature relating to the solid-like and liquid-like characters of the material can be indicated with the rate and the extent to which the deformation recovers on the elimination of the shear stress. The creep compliance ($J(t)$) of the ink variants, as the recoverable strain, could be obtained from the maximum point of deformation before the load is removed and the extent of deformation after the recovery period. The creep recovery curve provides several parameters, though in the present work, maximum $J(t)$ and relative recovery parameters were extracted. Previously, the printable inks with a higher amount of AMCC offered greater elasticity moduli and more shear-thinning behavior compared to samples with a lower micro-

biosurfactant content as revealed by the rheological experiments. Furthermore, the greater AMCC levels showed a desired thermo-reversible feature, suggesting stronger structural interactions associated with the resistance to diverse temperature processes. As depicted in Fig. 3b, the creep compliance extents of inks prepared by 3.15 and 4.2 wt% AMCC were lower than those made by 1.05 and 2.1 wt% micro-biosurfactant. Generally, the peak creep compliance for PEC3 ($J(t) = 0.32 \text{ Pa}^{-1}$) and PEC4 ($J(t) = 0.17 \text{ Pa}^{-1}$) was about 30- and 56-fold lower than control ink ($J(t) = 9.6 \text{ Pa}^{-1}$), respectively. Compared to PEC3 and PEC4, a comparatively weaker structure of PEC1 ($J(t) = 1.8 \text{ Pa}^{-1}$) and PEC2 ($J(t) = 0.61 \text{ Pa}^{-1}$) was deduced from a relatively greater peak strain (Fig. 3b). Then, it seemed higher micro-biosurfactant ratios were able to more strongly enhance the elastic elements of the viscoelastic property, possibly due to the presence of higher hydrophobic/hydrophilic domains in the system. This provides a strong interaction with the comparable groups in the adjacent droplets. These results are also in agreement with the data obtained from the oscillatory test.

The recovery stage of the creep assessment is the magnitude of decreasing the material deformation after the elimination of stress. A larger relative recovery is associated with greater elasticity and a solid-like structure [37]. The relative recovery ability was improved with an increased level of AMCC in the casein-based ink. The recovery percentage of PEC3 and PEC4 inks was much higher compared to control ink (about 47%), suggesting an actual reinforcement of the ink system recovery. In this context, a premiere relative recovery of about 83% was noticed for PEC4, followed by PEC3 with a recovery percentage of 81%, suggesting an improved elasticity with an appropriate stable structure. This proposes the formation of a strengthened ink structure induced by the addition of greater AMCC levels. Compared to PEC3 and PEC4, the PEC1 and PEC2 revealed lower relative recovery with a percentage of 66% and 70%, respectively. As an important consequence, the creep-recovery experiment suggested the formation of a reversible network matrix in the reduced-fat inks with the restoration of their initial structures upon breakdown. Besides, the data obtained from creep recovery tests offered the micro-biosurfactant ratio affected the elastic and the viscous components of viscoelastic character in the Pickering emulsions, whose results were in accordance with the data of discussed oscillatory measurements.

3.2.7. The 3ITT assay

The thixotropic properties of injectable gels upon application of high-shear conditions can be promoted by the reformation of network structure to yield a self-supporting structure. This feature can reduce the force required to drive ink extrusion, avoiding discontinuities and inhibiting geometry instability [16]. In this regard, the 3ITT experiment is a valuable approach to perform a rapid deformation to simulate the influences of extrusion shearing force during printing and also handling steps of 3D printed architectures. Ideally, a material is considered as a preferred thixotropic system if the peak viscosity in the third interval recovers at least 70% of its amount obtained after the initial interval [37]. The viscosity profiles of Pickering emulsions as a function of applied deformation rate and time are shown in Fig. 3c. In general, the viscosity of inks prepared with higher AMCC concentrations showed greater values in the first interval as expected, denoting a reinforcement of the structural strength. In this phase, PEC3 and PEC4 inks exhibited a substantially greater viscosity compared to PEC1 and PEC2. Relating to the third phase, the viscosity of reduced-fat ink variants was somewhat lower than those for the first stage. In the 3-ITT test, when the shear rate sharply steps up or down, the resulting viscosity transients reveal the alterations in the system structure under well-controlled flow conditions. Therefore, the viscosity for the ink systems upon stepwise shear rate was associated with its recovery compliance and viscoelasticity interval [37]. In the second interval, a large number of interconnected structures in the system were degraded, resulting in a considerable reduction of viscosity. When approached to the reversible

restructuring (*i.e.*, the third interval), the biopolymeric chains re-ordered as the structure came to the new equilibrium phase, recovering its initial structure. As visualized from Fig. 3c, the PEC3 and PEC4 inks exposed the superior structural recovery, in which the initial viscosity recovery was determined to be 76% and 85%, respectively. This could be attributed to the strengthening of the ink structure offered by higher levels of AMCC, allowing the resistance of the system to the prompt shear strain. Contrarily, the lower values of viscosity recovery of PEC1 (64%) and PEC2 (70%) might be due to some extent of irreversible structural damage. This proposed a soft matrix on account of the presence of less structured emulsions with the low-connected system. These outcomes were also consistent with the steady flow curve and oscillatory measurements, where the more structured Pickering emulsions exhibited a strong gel-like structure. Accordingly, the reduced-fat ink networks containing higher micro-biosurfactant contents (*i.e.*, PEC3 and PEC4) were dynamic and recoverable, and as a consequence, their suitability could be considered to be processed via 3D extrusion printer as restoration networks with reversible structure breakdown are highly desired.

3.2.8. LAOS behavior

The LAOS analysis can be used to study the structure-related rheological behavior under large deformations. It provides the visual difference in the nonlinear stress response (*i.e.*, strains beyond the LVR) on the complex microstructure of material that cannot be attained by the traditional rheological measurements [37]. Therefore, it can offer a rapid determination concerning actual physical processes responsible for microstructure collapse and structure evolution of systems under large deformations during 3D printing processing. In this context, the Lissajous-Bowditch curve obtained from LAOS analysis proposes the imperative information towards the structural transition with consideration of quantifying viscoelastic moduli outside the LVR, which is closer to the 3D printing process and application conditions. Additionally, LAOS's data can also contribute to the deduction of material behaviors upon oral processing, where its results are associated with the sensory and textural features of food [38]. The nonlinear character can be assessed through the magnitude and type of distortion of the Lissajous-Bowditch plots from an elliptical geometry. The Lissajous-Bowditch plots of printable ink variants at different amplitude and frequencies inside and beyond the LVR are illustrated in Fig. 4. The elliptical geometry of the Lissajous-Bowditch curves for all inks at 0.5% amplitude rate (inside the LVR) showed an elliptical shape. This reveals a linear viscoelastic response on account of biopolymeric chain viscoelasticity, as expected according to the strain sweep results (Fig. 2b). At the higher amplitudes and frequencies, the shapes of Lissajous-Bowditch plots from an ellipse converted to a non-elliptical (parallelogram) geometry, implying a nonlinear response (Fig. 4). The particular distortion is ascribed to different microstructural features and the development of shear-induced structures. This specifies increased viscous dissipation and a move from solid-dominated to the liquid-dominated character [32]. The obtained nonlinear property at the greater amplitudes could be probably caused by microstructural deformations, resulting in permanent flow and deformation.

The phase angle values at different strains and frequencies could show a change from elastic- to the viscous-prevalent characters through LAOS analysis (Table 2). With the increasing frequency at each strain, the phase angle was significantly increased ($P < 0.05$). Whereas the phase angle increased with increasing the amplitude, the magnitude of this increase was related to the micro-biosurfactant ratio. Within this framework, the printable inks prepared with 3.15 and 4.2 wt% AMCC (*i.e.*, PEC3 and PEC4) presented the lowest phase angle values at 0.5% strain, proposing a more prevail-elastic character and greater resistance to deformation (disruption) inside the LVR. As the oscillatory results indicated, the PEC3 and PEC4 inks revealed a higher network extension with greater dynamic moduli within the LVR (Sections 3.3 and 3.5).

The differences in the polymeric flexibility, stabilization mechanisms, and structural properties of interfacial layers can explain the

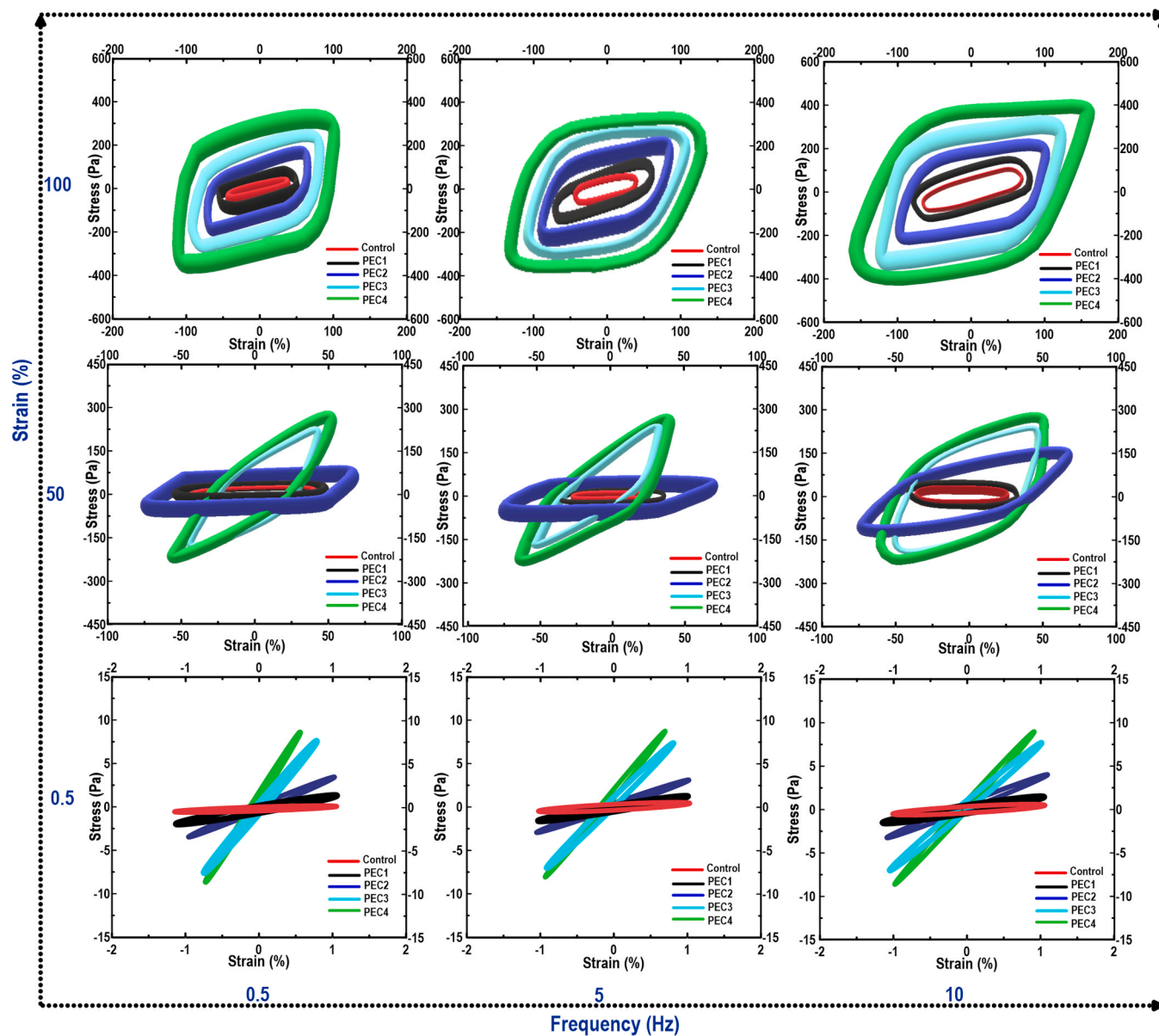


Fig. 4. The area is surrounded by the Lissajous-Bowditch plots as a function of amplitude and frequency in printable Pickering emulsion variants.

Table 2
Phase angles under LAOS for different printable Pickering emulsion inks.

Frequency (Hz)	Strain (%)	Control ^a	PEC1	PEC2	PEC3	PEC4
0.5	0.5	3.22 ± 0.011 ^d	3.49 ± 0.023 ^c	3.01 ± 0.032 ^c	2.64 ± 0.046 ^b	2.09 ± 0.021 ^a
	50	12.12 ± 0.034 ^a	18.38 ± 0.054 ^b	29.61 ± 0.062 ^c	33.57 ± 0.052 ^d	30.26 ± 0.046 ^e
	100	81.23 ± 0.078 ^a	88.43 ± 0.045 ^b	128.44 ± 0.097 ^c	163.22 ± 0.123 ^d	191.18 ± 0.145 ^e
5	0.5	5.19 ± 0.013 ^c	5.03 ± 0.012 ^d	4.62 ± 0.013 ^c	4.12 ± 0.017 ^b	3.69 ± 0.013 ^a
	50	14.55 ± 0.056 ^a	19.43 ± 0.066 ^b	32.57 ± 0.078 ^c	35.62 ± 0.052 ^d	37.76 ± 0.069 ^e
	100	83.49 ± 0.079 ^a	89.25 ± 0.084 ^b	130.00 ± 0.094 ^c	166.77 ± 0.099 ^d	192.84 ± 0.093 ^e
10	0.5	6.71 ± 0.018 ^e	6.36 ± 0.011 ^d	5.65 ± 0.017 ^c	5.02 ± 0.018 ^b	4.56 ± 0.023 ^a
	50	16.89 ± 0.053 ^a	20.89 ± 0.065 ^b	33.78 ± 0.077 ^c	37.33 ± 0.045 ^d	39.15 ± 0.076 ^e
	100	84.05 ± 0.087 ^a	90.23 ± 0.083 ^c	131.32 ± 0.154 ^c	168.50 ± 0.133 ^d	194.45 ± 0.131 ^e

^{a-e} Means (three replicates) within each column with different letters are significantly different ($P < 0.05$), Duncan's test.

^{*} Each row was considered to evaluate the significant differences.

changes in the phase angles of printable ink variants (Table 2) [38]. Although the steric or electrostatic repulsive effects and densely packed interface layer promoted a more solid-like behavior in PEC3 and PEC4 inks (see Sections 3.9 and 3.10), the presence of higher levels of particle-particle interactions reduced the network flexibility, leading to

larger structural damage upon the large deformation and greater viscous dissipation [39]. The dense matrix of PEC3 and PEC4 comprised a structured emulsion with greatly connected droplets and minimal inter-particle space. In this situation, there is no sufficient space for the droplets/particles to move freely under the application of higher strain

amplitudes. The failure of such a dense system to adjust to the large deformations led to a constant structural deformation and induction of viscous-like character. This is well supported by the strain sweep results, where the $G'(\gamma)$ trends of PEC3 and PEC4 inks presented much more sudden transitions (higher slope) from linear to nonlinear behavior as compared to the other inks.

Fig. 4 also proves that the reduced-fat inks offered larger nonlinearity at the higher frequencies, irrespective of amplitude. Though, the reduced-fat inks formulated by higher micro-biosurfactant levels presented less sensitivity to the frequency alterations inside LVR with more viscoelastic solid behavior and more structured systems. The greater relaxation in the reduced-fat inks could be possibly caused by the development of more intermolecular junctions in the Pickering emulsion and an improvement of network extension through steric or electrostatic repulsive interactions. This might also describe the lower extent of frequency-related changes of PEC3 and PEC4 inside LVR compared to other inks.

A third-order harmonic data to obtain the extent and type of nonlinear viscoelastic character can be utilized to quantitatively compare the nonlinear viscoelastic feature [40]. The magnitude of nonlinear viscoelastic character is determined through the proportion of the third harmonic viscoelastic moduli, G'_3 and G''_3 , to the first harmonic viscoelastic moduli, G'_1 and G''_1 . The extents of $G'_3 / G'_1 \geq 0.01$ and $G''_3 / G''_1 \geq 0.01$ specify the existence of nonlinear viscoelastic character, where the greater extents show the increased amount of nonlinear viscoelastic property. Besides, two viscoelastic moduli and two instantaneous viscosities show a particular type of nonlinear character [40]. The proportion of large-amplitude (G'_L) and minimum-amplitude elastic modulus (G'_M) can be employed to obtain the amplitude-softening ($G'_L / G'_M < 0.9$) and amplitude-hardening ($G'_L / G'_M > 1.1$) features. Likewise, the proportion of rapid viscosities at the maximum (η'_{L1}) and minimum shear rates (η'_{M1}) can be applied to measure the amount of shear-thinning ($\eta'_{L1} / \eta'_{M1} < 0.9$) and shear thickening characters ($\eta'_{L1} / \eta'_{M1} > 1.1$) (Tables 3 and 4).

The reduced-fat inks typically presented the linear viscoelastic character ($G'_3 / G'_1 < 0.01$, $0.9 < G'_L / G'_M < 1.1$) at a frequency of 0.5 Hz and 0.5% amplitude. At the higher strains and frequencies, both the extents of nonlinear behavior (G'_3 / G'_1 and G''_3 / G''_1 values) and amount of strain hardening ($G'_L / G'_M > 1.1$) and shear-thinning (η'_{L1} / η'_{M1} values) were increased with increasing the amplitude and frequency (Tables 3 and 4). These results are supported by Lissajous-Bowditch curves, dynamic rheological properties, and pseudoplasticity behavior obtained by the flow curve. From the third-order harmonic data, PEC3 and PEC4 inks presented a greater amount of nonlinear elastic character and smaller strain hardening at the frequencies and amplitudes higher than the LVR. These results are surprising according to the oscillatory rheological data. The nonlinear viscoelastic behaviors of PEC3 and PEC4 inks were anticipated to present a minor level of the nonlinear feature because of the high density of solid particles with a more close-packed,

strong solid-like structure, improved connected structure, and larger critical strain amounts. Furthermore, the strain-hardening behavior of PEC3 and PEC4 was expected to be larger than that of the other ink variants on account of more structured systems and stronger network structure. These results might be emanated from the increased network connectivity and contribution of micro-biosurfactant to promote stronger intermolecular interaction between the functional groups of AMCC and hydrophilic/hydrophobic domains of the casein/oil system. This makes PEC3 and PEC4 inks showed a solid microstructure with decreased flexibility, thicker interfacial layers, and a more compact gel structure compared to other Pickering emulsions. The firmer structure and densely packed layers provided by micro-biosurfactant at the higher ratios might be more possibly to deform upon LAOS, causing the droplets to slide past each other instead of rupture elastically. This led to decreased stored energy from the imparted amplitude and improved energy dissipation from the permanent deformation and viscous flow. Therefore, the degree of nonlinear character was still high but manifested as increased viscous-type behavior instead of increased elastic-type behavior, in agreement with the obtained results of third-order harmonic data.

3.2.9. Droplet size and zeta potential

The physicochemical characteristics of Pickering emulsions are affected by the biosurfactant ratio and its interactions at the O/W interface [29]. The effect of AMCC contents on the mean particle size of casein-based emulsion was characterized by the static light scattering (Fig. 5a). It is obvious that the $d_{(3,2)}$ and $d_{(4,3)}$ values were larger at day 21 compared to values of the first day, except for PEC3 and PEC4. Over 21 days of storage, the $d_{(3,2)}$ and $d_{(4,3)}$ of casein-based emulsion varied between 2 and 16 μm and 14–42 μm , respectively. In general, the $d_{(3,2)}$ and $d_{(4,3)}$ values were decreased as the AMCC level increased. The micro-biosurfactant could be dispersed well in the emulsion systems via hydrogen linkages and hydrophobic interaction, contributing to effectiveness on aging [41]. However, the existence of lower ratios of AMCC in the continuous phase was inadequate to generate high viscosities and developing a well-defined gel, which led to the larger flocculation among the droplets at the ratios of 1.05 and 2.1 wt% (Fig. 5a). The existence of flocculation and/or coalescence in the lower ratios of AMCC suggested the ability of micro-biosurfactant against the flocculation of the droplets was insufficient to offer emulsion stability over the storage. Contrarily, in the ranges of 3.15 and 4.2 wt% AMCC, the particle size of Pickering emulsion underwent a substantial reduction. This might be ascribed to the enhancement of the amount of adsorbed AMCC at the O/W interface and the existence of electrostatic repulsive interactions due to the addition of higher micro-biosurfactant levels. Furthermore, the emulsion stability could be associated with the formation of hydrogen linkages due to the interaction of amide, carboxylic, and hydroxyl groups of AMCC with casein, on one hand, and interaction of its acetyl domains with the oil phase. In summary, the levels of 3.15 and

Table 3
The elastic LAOS variables for printable inks prepared with different formulations.

ω (Hz)	γ (%)	Control*		PEC1		PEC2		PEC3		PEC4	
		G'_L / G'_M $\times (10)^{-2}$	$G'_3 / G'_1 \times (10)^{-3}$	$G'_L / G'_M \times (10)^{-2}$	$G'_3 / G'_1 \times (10)^{-3}$	$G'_L / G'_M \times (10)^{-2}$	$G'_3 / G'_1 \times (10)^{-3}$	$G'_L / G'_M \times (10)^{-2}$	$G'_3 / G'_1 \times (10)^{-3}$	$G'_L / G'_M \times (10)^{-2}$	$G'_3 / G'_1 \times (10)^{-3}$
0.5	0.5	99 ± 0.7 ^d	6 ± 0.01 ^d	99 ± 0.5 ^d	6 ± 0.01 ^d	97 ± 0.5 ^c	5 ± 0.01 ^c	95 ± 0.4 ^b	4 ± 0.01 ^b	91 ± 0.5 ^a	2 ± 0.01 ^a
	50	412 ± 2.1 ^d	33 ± 0.8 ^a	415 ± 2.7 ^d	34 ± 0.5 ^a	395 ± 2.3 ^c	37 ± 0.3 ^b	278 ± 2.1 ^b	55 ± 0.7 ^c	222 ± 1.7 ^a	64 ± 0.4 ^d
	100	1289 ± 5.8 ^d	34 ± 0.7 ^a	1298 ± 6.3 ^d	34 ± 0.4 ^a	1109 ± 4.9 ^c	39 ± 0.6 ^b	967 ± 4.5 ^b	58 ± 0.9 ^c	853 ± 3.1 ^a	69 ± 0.8 ^d
5	0.5	1.0 ± 0.1 ^e	4 ± 0.02 ^c	99 ± 0.1 ^d	4 ± 0.03 ^c	98 ± 0.4 ^c	4 ± 0.03 ^c	96 ± 0.6 ^b	3 ± 0.02 ^b	91 ± 0.7 ^a	2 ± 0.02 ^a
	50	490 ± 3.1 ^e	41 ± 0.3 ^a	476 ± 2.4 ^d	42 ± 0.7 ^a	433 ± 1.6 ^c	42 ± 0.6 ^a	293 ± 1.4 ^b	59 ± 0.3 ^b	256 ± 1.9 ^a	66 ± 0.9 ^c
	100	2989 ± 10.3 ^c	55 ± 0.09 ^a	3105 ± 11.1 ^d	56 ± 0.08 ^a	2851 ± 9.4 ^c	64 ± 0.08 ^b	1788 ± 7.8 ^b	75 ± 0.7 ^c	1506 ± 7.3 ^a	83 ± 0.8 ^d
10	0.5	1.0 ± 0.1 ^a	3 ± 0.02 ^c	1.0 ± 0.2 ^a	3 ± 0.01 ^c	99 ± 0.2 ^a	3 ± 0.03 ^c	97 ± 0.7 ^b	2 ± 0.01 ^b	93 ± 0.4 ^c	1 ± 0.04 ^a
	50	758 ± 4.6 ^c	48 ± 0.3 ^a	743 ± 6.2 ^d	50 ± 0.7 ^b	686 ± 5.3 ^c	50 ± 0.9 ^b	479 ± 2.9 ^b	65 ± 1.3 ^c	382 ± 3.1 ^a	74 ± 1.1 ^d
	100	3284 ± 17.0 ^e	59 ± 0.8 ^a	3118 ± 18.7 ^d	60 ± 1.1 ^a	2937 ± 15.1 ^c	66 ± 1.4 ^b	1875 ± 15.4 ^b	81 ± 1.8 ^c	1563 ± 14.1 ^a	89 ± 1.7 ^d

^{a-e} Means (three replicates) within each column with different letters are significantly different ($P < 0.05$), Duncan's test.

* Each row from comparable parameters was considered to evaluate the significant differences.

Table 4

The viscous LAOS variables for printable inks prepared with different formulations.

ω (Hz)	γ (%)	Control ^a		PEC1		PEC2		PEC3		PEC4	
		η'_{L} / η'_{M} $\times (10)^{-2}$	$G'_{3} / G'_{1} \times (10)^{-3}$	η'_{L} / η'_{M} $\times (10)^{-2}$	$G'_{3} / G'_{1} \times (10)^{-3}$	η'_{L} / η'_{M} $\times (10)^{-2}$	$G'_{3} / G'_{1} \times (10)^{-3}$	η'_{L} / η'_{M} $\times (10)^{-2}$	$G'_{3} / G'_{1} \times (10)^{-3}$	η'_{L} / η'_{M} $\times (10)^{-2}$	$G'_{3} / G'_{1} \times (10)^{-3}$
0.5	0.5	97 ± 0.5 ^c	5 ± 0.02 ^c	96 ± 0.6 ^c	5 ± 0.02 ^c	97 ± 0.7 ^c	5 ± 0.01 ^c	90 ± 0.5 ^b	3 ± 0.02 ^b	88 ± 0.8 ^a	1 ± 0.007 ^a
	50	87 ± 0.8 ^c	21 ± 0.5 ^a	88 ± 0.9 ^c	21 ± 0.6 ^a	85 ± 0.8 ^b	26 ± 0.2 ^b	82 ± 0.6 ^a	34 ± 0.4 ^c	83 ± 0.4 ^a	40 ± 0.6 ^d
	100	84 ± 1.2 ^c	23 ± 0.5 ^a	84 ± 0.5 ^c	26 ± 0.3 ^b	85 ± 0.8 ^c	30 ± 0.4 ^c	78 ± 0.6 ^b	39 ± 0.5 ^d	71 ± 0.9 ^a	46 ± 0.3 ^e
5	0.5	96 ± 0.2 ^c	4 ± 0.06 ^c	96 ± 1.0 ^c	4 ± 0.05 ^c	95 ± 0.9 ^c	4 ± 0.02 ^c	93 ± 0.4 ^b	2 ± 0.03 ^b	89 ± 0.7 ^a	1 ± 0.01 ^a
	50	89 ± 1.4 ^c	23 ± 0.5 ^a	90 ± 1.2 ^c	24 ± 0.2 ^a	87 ± 0.6 ^b	29 ± 0.5 ^b	84 ± 0.5 ^a	38 ± 0.4 ^c	84 ± 0.5 ^a	49 ± 0.6 ^d
	100	87 ± 0.4 ^c	24 ± 0.2 ^a	88 ± 0.7 ^c	29 ± 0.1 ^b	87 ± 1.2 ^c	31 ± 0.2 ^b	82 ± 1.4 ^b	41 ± 0.9 ^c	77 ± 2.2 ^a	54 ± 1.2 ^d
10	0.5	96 ± 0.4 ^c	2 ± 0.05 ^c	95 ± 0.7 ^c	2 ± 0.02 ^c	95 ± 1.1 ^c	2 ± 0.02 ^c	93 ± 0.2 ^b	1 ± 0.02 ^b	90 ± 0.6 ^a	0.8 ± 0.01 ^a
	50	92 ± 1.0 ^c	24 ± 0.3 ^a	93 ± 1.1 ^c	24 ± 0.5 ^a	90 ± 0.6 ^b	31 ± 0.2 ^b	89 ± 1.2 ^b	41 ± 0.7 ^c	85 ± 1.3 ^a	53 ± 0.7 ^d
	100	89 ± 1.2 ^{cd}	25 ± 0.4 ^a	90 ± 0.7 ^d	31 ± 0.7 ^b	88 ± 0.9 ^c	34 ± 0.5 ^c	85 ± 3.3 ^b	47 ± 0.6 ^d	81 ± 2.4 ^a	61 ± 0.5 ^e

^{a-e} Means (three replicates) within each column with different letters are significantly different ($P < 0.05$), Duncan's test.

^{*} Each row from comparable parameters was considered to evaluate the significant differences.

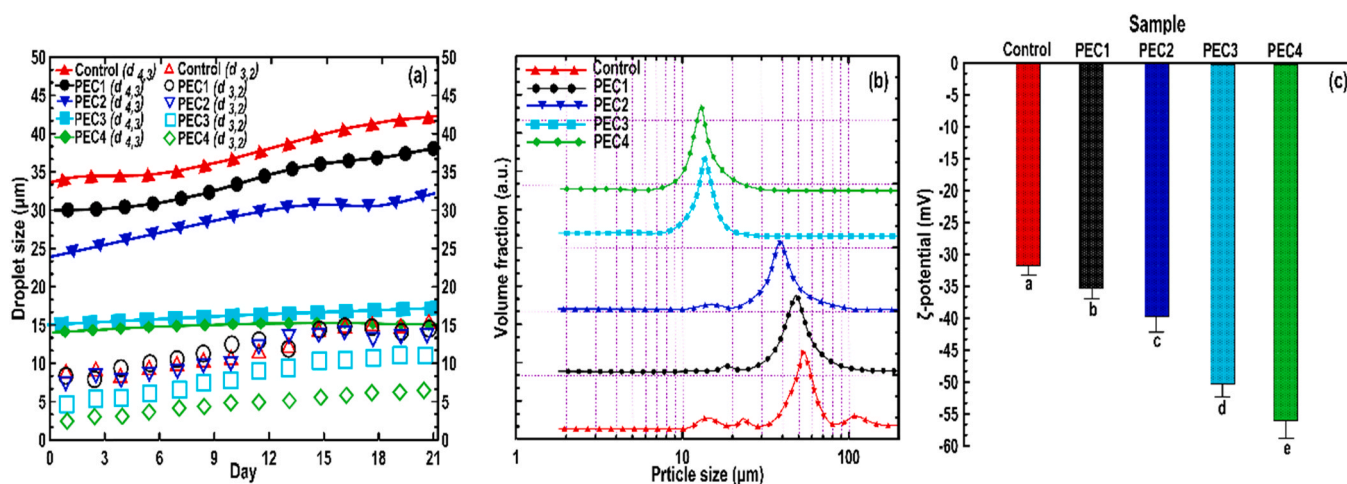


Fig. 5. Influence of AMCC ratios on droplet size (a), particle size distribution (b), and zeta potential (c) of casein-based Pickering emulsion.

4.2 wt% AMCC seemed to show a proper ability to stabilize the ink through thickening and formation of a three-dimensional network as supported by the rheological measurements.

The size distribution results of casein-based Pickering emulsion prepared by different AMCC ratios are presented in Fig. 5b. The control ink (with no micro-biosurfactant) allowed the development of aggregates and showed the multimodal distribution of particle size. The small protein/droplets aggregation was also observed in the inks with AMCC levels of 1.05 and 2.1 wt%. This offered a bimodal distribution and increased size diameter, where the maximum peak appeared at 37 (PEC1) and 46 μm (PEC2). On the other hand, when 3.15 and 4.2 wt% AMCCs were incorporated into the system, the minor peak related to the aggregated droplets was disappeared and a reduction in the fraction of larger particles was detected (Fig. 5b). In this sense, the PEC3 and PEC4 inks showed a stable system characterized by monomodal distribution. This presents no stable flocs were identified upon the PSD experiment, suggesting better emulsion stability. From these results, it is evident the casein-based ink needed a high ratio of micro-biosurfactant to develop a stable system with monomodal distribution and minimum size diameter ($< 20 \mu\text{m}$). It could also be seen the PSD data were in agreement with results of $d(3,2)$ and $d(4,3)$. The better emulsifying capacity offered by the greater micro-biosurfactant content could be attributed to the existence of higher numbers of acetyl headgroup to interact with oil and larger amounts of cellulose backbone to involve with the hydrophilic groups of casein. This allows the necessary interfacial free energy to inhibit the system destabilization and further phase separation. Additionally, the enhanced homogeneity and more uniform particle size distribution provided by higher AMCC levels could be likely related to an increase in the oil droplet's surface coverage, exhibiting the

interfacial adhesion between micro-biosurfactant and hydrophobic phase. These results support the former interpretation on the stabilizing effect of AMCC due to viscosity improvement of the continuous phase and/or formation of more intermolecular junctions in the system.

The zeta (ζ) potential is a physicochemical factor of specific significance in portraying surface electrical properties of charged media, which is a useful parameter for determining the electro-kinetic surface properties of both pristine and modified surfaces. Since the electrostatic repulsive force acts as one of the imperative interactions in avoiding the aggregation of casein-based emulsion, the ζ -potential of inks prepared with different ratios of AMCC was obtained (Fig. 5c). The ζ -potential of the casein-coated droplets in control ink was determined to be -32.1 mV (pH 7.0), which was expected as the caseins at the pH higher than its isoelectric point (about 4.5) are negatively charged [42]. The data obtained also revealed that the ζ -potential of particles stabilized by the lower levels of micro-biosurfactant, i.e., 1.05 and 2.1 wt% AMCC, was -36.6 to -39.1 mV , respectively. The small increase in the ζ -potential (more negative) of PEC1 and PEC2 indicated that electrostatic repulsion in the system is moderately present due to the incorporation of more negatively charged groups into the system. On the other hand, the negative ζ -potential more increased when AMCC was added at the ratios of 3.15 (-50.2 mV) and 4.2 wt% (-56.8 mV). This indicates the electrostatic repulsive forces of PEC3 and PEC4 were stronger compared to the rest of Pickering emulsions. As acetylated MCC is negatively charged, the negative ζ -potential was increased with an increase of the AMCC ratio in the system. This represents good protection against droplet aggregation on account of a combination of electrostatic and steric stabilization. Xu et al. [7] also reported that the negative charge of the droplets was increased after MCC addition.

3.2.10. Ink microstructure

The CLSM is an efficient tool to examine the real distributions and interactions between colloidal particles, in which it provides the network structure and interfacial framework in the continuous phase of Pickering emulsions. The photomicrograph of the ink in the absence of micro-biosurfactant presented the existence of large droplets with rather small spaces between them, whereas the quite small oil droplets were detected in the samples with the higher ratios of AMCC (Fig. 6). The observed instability regarding control ink could be owing to the lack of micro-biosurfactant presented at the created O/W interface for surface coverage. Therefore, the flocculation and coalescence of droplets became possible. Regarding reduced-fat inks, the CLSM micrographs clearly showed the adsorption of AMCC/casein protein on the droplet surface. The fluorescence images of the reduced-fat inks also exposed the oil phase located in the interior of the globules, where the yellow bright AMCC/casein was visualized at the boundary of droplets. The AMCC at the higher ratios developed a densely packed layer on the surface of spherical oil droplets. This interfacial structure offered a solid barrier for Pickering emulsions, which enhanced the storage stability against coalescence, flocculation, and Ostwald ripening. Remarkably, a denser on-adsorbed AMCC (and casein) network structure was developed with increased AMCC levels. This provided the depletion flocculation through the osmotic pressure gradient inside the continuous phase surrounding the droplets and their subsequent aggregation would lead to stronger

interactions among droplets [29]. Moreover, the droplets in the PEC3 and PEC4 inks dispersed more regularly in the continuous phase with a smaller size. It was stated that modified cellulose can offer superior emulsion stability against coalescence and flocculation due to irreversible adsorption at the O/W [41,43]. It can be concluded then that the casein-based emulsions stabilized by the higher levels of AMCC showed the smaller and non-aggregated droplets, which were homogeneously distributed throughout the continuous phase.

4. Conclusion

The findings of this study offered a deeper understanding of the role of Pickering emulsion in the structuring of the reduced-fat casein-based emulsion with consideration of acetylated microcrystalline cellulose functionality. The produced Pickering emulsion provided desirable *pseudoplasticity*, viscoelasticity, droplet size, and thixotropic behavior with a reversible dynamic matrix, especially at the higher ratios of micro-biosurfactant. These results suggested that casein-based ink, in the form of Pickering emulsion, may show potential as a sustainable printable ink processable for the 3D printing application. The rheological experiment exposed that the micro-biosurfactant ratio influenced the flow behavior of the emulsion, enhancing its shear-thinning character and increasing yield stress and consistency index. The reduced-fat casein-based emulsions also displayed structural stability when a temperature ramp was applied. The thixotropic data revealed that the reduced-fat inks presented an increased degree of recovery yield and larger resistance to the deformation with the formation of a reversible network. A higher ratio of micro-biosurfactant led to an improvement of emulsion stability during storage, as indicated by smaller oil droplet size with the monomodal distribution. The reduced-fat casein-based emulsions also caused a larger amount of nonlinear behavior and increased shear-thinning under large amplitude oscillatory shear stress, but higher critical strain, and higher moduli values in the linear viscoelastic region. These stability differences will probably contribute to differences in the textural and structural behaviors of Pickering emulsion under the 3D printing process.

Compliance with ethics requirements

The authors declare no conflict of interest.

Funding

Open access funding provided by the University of Natural Resources and Life Sciences Vienna (BOKU).

CRediT authorship contribution statement

Mahdiyar Shahbazi: Conceptualization, Methodology investigation, Collecting data, Validation, Data interpretation, Funding acquisition, Writing - original draft, Writing - review & editing. **Henry Jäger:** Methodology, Writing - review & editing, Supervision. **Rammile Ette-laie:** Writing - review & editing.

Declaration of Competing Interest

The authors declare that they have no known competing financial interests or personal relationships that could have appeared to influence the work reported in this paper.

Appendix A. Supporting information

Supplementary data associated with this article can be found in the online version at [doi:10.1016/j.colsurfa.2021.126641](https://doi.org/10.1016/j.colsurfa.2021.126641).

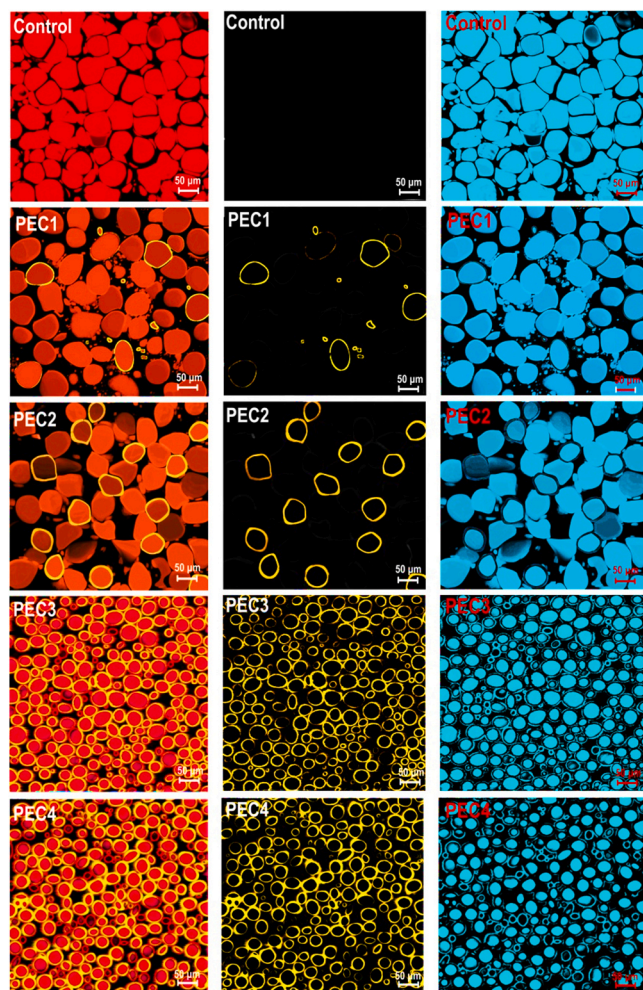


Fig. 6. CLSM images of casein-based Pickering emulsion stabilized by different ratios of AMCC. Oil phase (right column) (for better clarification the red color was changed to cyan color), AMCC/casein stained yellow (middle column), and overlapping images (left column).

References

- [1] H.P. Bachmann, Cheese analogues: a review, *Int. Dairy J.* 11 (4–7) (2001) 505–515.
- [2] B.B. Mulsow, D. Jaros, H. Rohm, Processed cheese and cheese analogues, *Struct. Dairy Prod.* 1 (2007) 210–235.
- [3] L.L. Ferrão, E.B. Silva, H.L.A. Silva, R. Silva, N. Mollakhalili, D. Granato, A.G. Cruz, Strategies to develop healthier processed cheeses: reduction of sodium and fat contents and use of prebiotics, *Food Res. Int.* 86 (2016) 93–102.
- [4] P. Tingaut, T. Zimmermann, G. Sèbe, Cellulose nanocrystals and microfibrillated cellulose as building blocks for the design of hierarchical functional materials, *J. Mater. Chem.* 22 (38) (2012) 20105–20111.
- [5] E. Dickinson, Biopolymer-based particles as stabilizing agents for emulsions and foams, *Food Hydrocoll.* 68 (2017) 219–231.
- [6] M. Gibis, V. Schuh, J. Weiss, Effects of carboxymethyl cellulose (CMC) and microcrystalline cellulose (MCC) as fat replacers on the microstructure and sensory characteristics of fried beef patties, *Food Hydrocoll.* (2015) 236–246.
- [7] D. Xu, J. Zhang, Y. Cao, J. Wang, J. Xiao, Influence of microcrystalline cellulose on the microrheological property and freeze-thaw stability of soybean protein hydrolysate stabilized curcumin emulsion, *LWT-Food Sci. Technol.* 66 (2016) 590–597.
- [8] A. Zbikowska, M. Kowalska, J. Pieniowska, Assessment of shortcrust biscuits with reduced-fat content of microcrystalline cellulose and psyllium as fat replacements, *J. Food Process. Preserv.* 42 (8) (2018), e13675.
- [9] N. Lin, J. Huang, P.R. Chang, J. Feng, J. Yu, Surface acetylation of cellulose nanocrystal and its reinforcing function in poly (lactic acid), *Carbohydr. Polym.* 83 (4) (2011) 1834–1842.
- [10] R.D. Kale, V.G. Gorade, N. Madye, B. Chaudhary, P.S. Bangde, P.P. Dandekar, Preparation and characterization of biocomposite packaging film from poly (lactic acid) and acylated microcrystalline cellulose using rice bran oil, *Int. J. Biol. Macromol.* 118 (2018) 1090–1102.
- [11] J.A.Á. Ramírez, C.J. Suriano, P. Cerrutti, M.L. Foresti, Surface esterification of cellulose nanofibers by a simple organocatalytic methodology, *Carbohydr. Polym.* 114 (2014) 416–423.
- [12] C. Le Tohic, J.J. O'Sullivan, K.P. Drapala, V. Chartrin, T. Chan, A.P. Morrison, A. L. Kelly, Effect of 3D printing on the structure and textural properties of processed cheese, *J. Food Eng.* 220 (2018) 56–64.
- [13] C. Kern, J. Weiss, J. Hinrichs, Additive layer manufacturing of semi-hard model cheese: effect of calcium levels on thermo-rheological properties and shear behavior, *J. Food Eng.* 235 (2018) 89–97.
- [14] K. Daffner, S. Vadodaria, L. Ong, S. Nöbel, S. Gras, I. Norton, T. Mills, Design and characterization of casein-whey protein suspensions via the pH-temperature-route for application in extrusion-based 3D-printing, *Food Hydrocoll.* 112 (2021), 105850.
- [15] M.A.I. Schutyser, S. Houlder, M. de Wit, C.A.P. Buijsse, A.C. Alting, Fused deposition modelling of sodium caseinate dispersions, *J. Food Eng.* 220 (2018) 49–55.
- [16] M. Shahbazi, H. Jäger, Current status in the utilization of biobased polymers for 3D printing process: a systematic review of the materials, processes, and challenges, *ACS Appl. Bio Mater.* (2020).
- [17] Y. Chevalier, M.A. Bolzinger, Emulsions stabilized with solid nanoparticles: Pickering emulsions, *Colloids Surf. A: Physicochem. Eng. Asp.* 439 (2013) 23–34.
- [18] L. Li, Y. Chen, T. Yu, N. Wang, C. Wang, H. Wang, Preparation of polylactic acid/TEMPO-oxidized bacterial cellulose nanocomposites for 3D printing via Pickering emulsion approach, *Compos. Commun.* 16 (2019) 162–167.
- [19] Y. Hu, J. Wang, X. Li, X. Hu, W. Zhou, X. Dong, B.P. Binks, Facile preparation of bioactive nanoparticle/poly (ε-caprolactone) hierarchical porous scaffolds via 3D printing of high internal phase Pickering emulsions, *J. Colloid Interface Sci.* 545 (2019) 104–115.
- [20] J. Wang, H. Gao, Y. Hu, N. Zhang, W. Zhou, C. Wang, Z. Yang, 3D printing of Pickering emulsion inks to construct poly (D, L-lactide-co-trimethylene carbonate)-based porous bioactive scaffolds with shape memory effect, *J. Mater. Sci.* 56 (1) (2020) 731–745.
- [21] T.A. Dankovich, Y.L. Hsieh, Surface modification of cellulose with plant triglycerides for hydrophobicity, *Cellulose* 14 (5) (2007) 469–480.
- [22] M. Shahbazi, G. Rajabzadeh, A. Rafe, R. Ettelaie, S.J. Ahmadi, Physico-mechanical and structural characteristics of blend film of poly (vinyl alcohol) with biodegradable polymers as affected by disorder-to-order conformational transition, *Food Hydrocoll.* 71 (2017) 259–269.
- [23] M. Shahbazi, G. Rajabzadeh, A. Rafe, R. Ettelaie, S.J. Ahmadi, The physico-mechanical and structural characteristics of blend film of poly (vinyl alcohol) with biodegradable polymers as affected by disorder-to-order conformational transition, *Food Hydrocoll.* 60 (2016) 393–404.
- [24] S. Park, J.O. Baker, M.E. Himmel, P.A. Parilla, D.K. Johnson, Cellulose crystallinity index: measurement techniques and their impact on interpreting cellulase performance, *Biotechnol. Biofuels* 3 (1) (2010) 10.
- [25] ASTM D871-96 Stand. Test. Methods Test. Cellul. acetate (Solut. Method; Proced. A) 2004.
- [26] M. Kiumarsi, D. Majchrzak, S. Yeganehzad, H. Jäger, M. Shahbazi, Comparative study of instrumental properties and sensory profiling of low-calorie chocolate containing hydrophobically modified inulin. Part I: rheological, thermal, structural and external preference mapping, *Food Hydrocoll.* 104 (2020), 105698.
- [27] W.L. Earl, D.L. VanderHart, High resolution, magic angle sampling spinning carbon-13 NMR of solid cellulose I, *J. Am. Chem. Soc.* 102 (9) (1980) 3251–3252.
- [28] R.H. Newman, Carbon-13 NMR evidence for cocrystallization of cellulose as a mechanism for hornification of bleached kraft pulp, *Cellulose* 11 (1) (2004) 45–52.
- [29] D.J. McClements, *Food Emulsions: Principles, Practices, and Techniques*, CRC Press, 2015.
- [30] M. Kiumarsi, D. Majchrzak, H. Jäger, J. Song, O. Lieleg, M. Shahbazi, Comparative study of instrumental properties and sensory profiling of low-calorie chocolate containing hydrophobically modified inulin. Part II: proton mobility, topological, tribological and dynamic sensory properties, *Food Hydrocoll.* 110 (2021), 106144.
- [31] H.A. Barnes, J.F. Hutton, K. Walters, *An Introduction to Rheology*, Elsevier, 1989.
- [32] K. Hyun, M. Wilhelm, C.O. Klein, K.S. Cho, J.G. Nam, K.H. Ahn, S.J. Lee, R. H. Ewoldt, G.H. McKinley, A review of nonlinear oscillatory shear tests: Analysis and application of large amplitude oscillatory shear (LAOS), *Prog. Polym. Sci.* 36 (12) (2011) 1697–1753.
- [33] M. Shahbazi, H. Jäger, S.J. Ahmadi, M. Lacroix, Electron beam crosslinking of alginate/nanoclay ink to improve functional properties of 3D printed hydrogel for removing heavy metal ions, *Carbohydr. Polym.* 240 (2020), 116211.
- [34] H.C. Mahler, W. Friess, U. Grauschopf, S. Kiese, Protein aggregation: pathways, induction factors and analysis, *J. Pharm. Sci.* 98 (9) (2009) 2909–2934.
- [35] K. Samejima, M. Ishioroshi, T. Yasui, Relative roles of the head and tail portions of the molecule in heat-induced gelation of myosin, *J. Food Sci.* 46 (5) (1981) 1412–1418.
- [36] M. Panouillé, T. Nicolai, D. Durand, Heat induced aggregation and gelation of casein submicelles, *Int. Dairy J.* 14 (4) (2004) 297–303.
- [37] K.P. Menard, N. Menard, *Dynamic mechanical analysis. Encyclopedia of Analytical Chemistry: Applications, Theory and Instrumentation*, John Wiley & Sons, Ltd., 2006, pp. 1–25.
- [38] H.S. Melito, C.R. Daubert, E.A. Foegeding, Relating large amplitude oscillatory shear and food behavior: correlation of nonlinear viscoelastic, rheological, sensory and oral processing behavior of whey protein isolate/κ-carrageenan gels, *J. Food Process Eng.* 36 (4) (2013) 521–534.
- [39] H.S. Joyner, A. Meldrum, Rheological study of different mashed potato preparations using large amplitude oscillatory shear and confocal microscopy, *J. Food Eng.* 169 (2016) 326–337.
- [40] R.H. Ewoldt, A.E. Hosoi, G.H. McKinley, New measures for characterizing nonlinear viscoelasticity in large amplitude oscillatory shear, *J. Rheol.* 52 (6) (2008) 1427–1458.
- [41] E. Dickinson, Use of nanoparticles and microparticles in the formation and stabilization of food emulsions, *Trends Food Sci. Technol.* 24 (1) (2012) 4–12.
- [42] D.G. Dalgleish, On the structural models of bovine casein micelles—Review and possible improvements, *Soft Matter* 7 (6) (2011) 2265–2272.
- [43] H.M. Ahsan, X. Zhang, Y. Li, B. Li, S. Liu, Surface modification of microcrystalline cellulose: physicochemical characterization and applications in the stabilization of Pickering emulsions, *Int. J. Biol. Macromol.* 132 (2019) 1176–1184.